Use of Remote Imagery to Map Microbialite Distribution at Great Salt Lake, Utah: Implications for Microbialite Exposure

Laura Wilcock[1,2], Carie M. Frantz[1], and Michael D. Vanden Berg[3]

[1]*Department of Earth & Environmental Sciences, Weber State University, Ogden, Utah; Laura.wilcock@utah.edu*

[2]*Department of Geology and Geophysics, University of Utah, Salt Lake City, Utah*

[3]*Energy & Minerals Program, Utah Geological Survey, Salt Lake City, Utah*

10.31711/ugap.v51i.136

ABSTRACT

The elevation of Great Salt Lake has fallen to historic lows in recent years, exposing once submerged microbialites along the lake's shores. Although prior studies have attempted to map microbialite locations, this has proved challenging, with mapped microbialite areas limited to accessible shoreline locations or via indirect sonographic evidence. Meanwhile, the importance of Great Salt Lake's microbialites to the lake's food chain has made quantifying the extent of microbialites exposed versus submerged at different lake elevations critical to lake management decisions. Low lake levels combined with seasonal high-water clarity have enabled microbialite reefs to be spotted in aerial and satellite imagery, even in deeper areas of the lake. In this study, satellite images were used to identify and map microbialite reef areas in Great Salt Lake and along its dry shores. In the south arm, submerged microbialites were easily recognized as dark green reefs against a light-colored benthic background (primarily ooid sand). Stationary microbialite mounds were distinguished from rip-up clasts or other dark-colored mobile material by comparing potential microbialite regions across several high-visibility timepoints. In this way, we identified 649 km^2 (251 mi^2) of putative microbialite reef area: 288 km^2 (111 mi^2) in the north arm, 360 km^2 (139 mi^2) in the south arm, of which 375 km^2 (145 mi^2) was mapped at a high degree of confidence. We also produced geospatial shapefiles of these areas. This map, combined with currently available lake bathymetric data, permits the estimation of the extent of microbialite reef exposed vs. submerged in various parts of the lake at different lake elevations. At the end of fall 2022, when lake level dipped to 1276.7 masl (4188.5 ft-asl) in elevation, we estimate that ~40% of the south arm microbialite reef area was exposed.

INTRODUCTION

Microbialites cover substantial portions of the Great Salt Lake benthos, and host microbial communities are believed to be important to the Great Salt Lake ecosystem. Models of the lake's ecosystem, therefore, must necessarily incorporate estimates of microbialite extent (Belovsky and others, 2011; Barrett, 2020), which need refining, particularly in the face of recent lake level decline and microbialite exposure.

Microbialites in Modern Great Salt Lake

Great Salt Lake is the largest saline lake in the western hemisphere. Unlike other terminal lakes in the Basin and Range of the western United States, which tend to be alkaline, Great Salt Lake is a Na-Mg-Cl-SO_4-dominated system with relatively low levels of alkalinity (Domagalski and others, 1989; Jones and others, 2009). High rates of Ca^{2+} and HCO_3^- delivery, slightly alkaline surface waters, the lake's hypersalinity (which promotes CO_2 degassing), and high levels of microbial activity produce conditions that approach or exceed aragonite saturation in much of the lake, despite relatively low lake water concentrations of Ca^{2+} and CO_3^- (Pace and others, 2016; Ingalls and others, 2020; Bouton and others, 2020). These factors have made Great Salt Lake (as well as its predecessors) a "carbonate factory," with carbonates making up a major portion of lake sediments, especially since the draining of Pleistocene Lake Bonneville (Jones and others, 2009; Vennin and others, 2019). Carbonate deposits blanket the modern bed of the lake, and include organic-rich carbonate mud, oolitic sand, and microbialite reefs (Eardley, 1938; Chidsey and others, 2015; Vanden Berg, 2019; Ingalls and others, 2020; Bouton and others, 2020; Baskin and others, 2022).

Microbialites are "organosedimentary deposits formed from interaction between benthic microbial communities…and detrital or chemical sediment" (Burne and Moore, 1987). They are typically formed by processes of trapping and binding by microbial mats (for example, Frantz and others, 2015),

induction of mineral precipitation via metabolic activities of microbial communities (for example, Dupraz and others, 2009), and/or inorganic calcification (for example, Shen and others, 2022). An aside on terminology: the term "bioherm," ostensibly coined by Cumings and Shrock (1928), broadly refers to any reeflike mound built by living organisms. "Microbialite," meanwhile, refers to a sedimentary rock built at least in part by the activities of microorganisms (Burne and Moore, 1987). Thus, "microbialite reef" is subtly different from "bioherm," indicating that microorganisms are involved in the construction of the reefs, but also acknowledging potential abiogenic contributions.

Great Salt Lake's microbialites were first documented by Eardley (1938) in his seminal tome describing the lake's chemistry and sediments, describing in detail the "extensive calcareous bioherms" that were visible during a period of relatively low lake elevation in the mid-1930s (Figure 1). He noted their dense mats (periphyton), dominated by the cyanobacterium *Aphanothece packardii* (now identified as *Eu-*

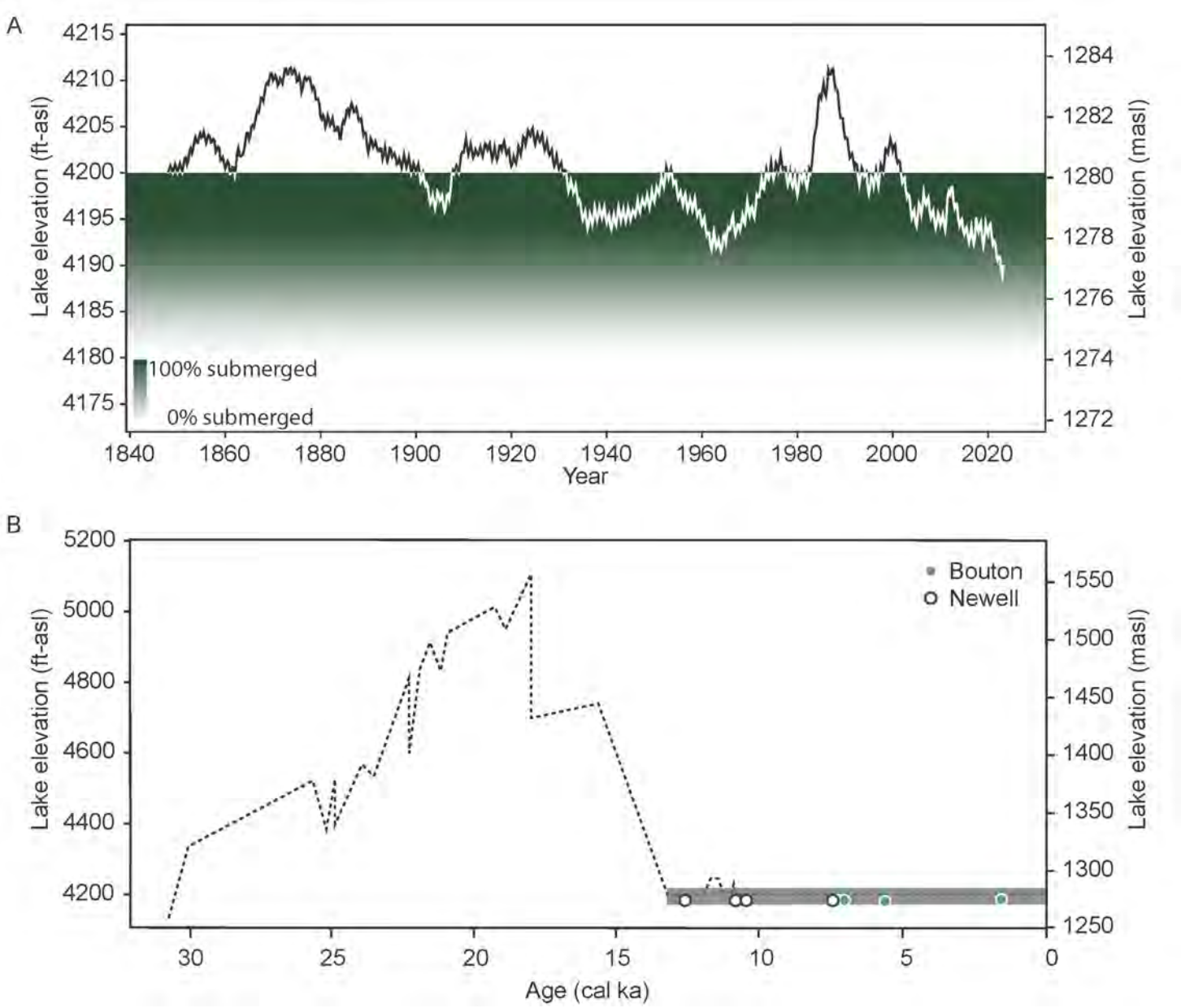

Figure 1. *A) Modern Great Salt Lake south arm surface elevations as measured at USGS water monitoring locations 1001000 and 10010024. Green shaded areas indicate 1 ft elevation bands below 4200 ft-asl where microbialites were mapped (this study), with shade indicating the total percentage of microbialites that would be submerged at that lake elevation. B) Lake Bonneville-Great Salt Lake hydrograph (black line) showing ages and elevations of dated microbialite materials from Bouton and others, 2016a (light green circles) and Newell and others, 2017 (dark green circles). Hydrograph prior to 13 ka modeled after Oviatt, 2015. Hydrograph after 13 ka modeled after Oviatt and others, 2021, with the dark gray horizontal bar indicating the uncertainty in lake elevation during the Great Salt Lake phase.*

halothece spp.; Lindsay and others, 2019; Frantz and others, 2023), and attributed their formation to microbially-mediated carbonate precipitation.

Even lower lake elevations in the early 1960s afforded a second look at the lake's microbialites. Carozzi (1962) examined their morphological variability and spatial distribution and linked their occurrence to underlying topographic highs. Halley (1976) described in detail the high variability in their internal structure, with laminated and unlaminated microfabrics existing within different portions of single microbialites (hence, "microbialite" vs. a more descriptive term such as thrombolite or stromatolites). He also noted a general lack of relationship between the living periphyton and observed calcified microstructure and microfossils, notably remarking that, "the organisms on the surface of the Great Salt Lake algal mounds are probably not those which are responsible for the internal structure."

By the late 1960s, the lake's microbialites were once again submerged by a rise in lake level and all but forgotten until they reappeared in the early 2010s during the period of prolonged lake level fall after the 1986–1987 lake highstand. This ushered in a new era of Great Salt Lake microbialite research in which the microbialites were investigated as contributors to the lake ecosystem (Wurtsbaugh, 2009; Belovsky and others, 2011; Wurtsbaugh and others, 2011) and as geobiologic curiosities (Pedone and Folk, 1996; Baskin, 2014; Pace and others, 2016; Lindsay and others, 2017). Interest in the structures was further enhanced by the discovery of the microbialite-associated pre-salt petroleum deposits of offshore Brazil in the mid-2000s, with interest in Great Salt Lake as a potential modern analog environment (Chidsey and others, 2015; Vanden Berg, 2019). Recent studies utilized new techniques and technology, including advanced microscopy (Pace and others, 2016), molecular biology (Lindsay and others, 2017), geospatial and marine acoustic technology (Baskin, 2014; Baskin and others, 2022), and drone imagery (Vanden Berg, 2019).

While the bulk of academic focus on the lake's microbialites (including that of this paper) has been on the extensive reefs that are submerged during "normal" levels of the modern lake, i.e., those below about 1280 meters above sea level (masl; 4200 feet above sea level, or ft-asl), microbialites and other putative microbial carbonates are also found in discrete locations at higher elevations, associated with earlier phases of the lake system (Chidsey and others, 2015; Vennin and others, 2019; Homewood and others, 2022). However, in the remainder of this paper, we use "microbialites" to refer only to the reef-forming deposits below 1280 masl (4200 ft-asl) in Great Salt Lake and its recently exposed shores.

The mega- and macrostructure (Shapiro, 2000) of Great Salt Lake's microbialites includes roughly circular domes ranging in size from ~15–300 cm in diameter, rings of the same scale with collapsed interiors, linear ridges up to several meters long, and mounds that outline the cracks of 30–75 m desiccation polygons at the lake margin (Vanden Berg, 2019) (Figure 2). The morphological diversity of the microbialites is presumably influenced by physical factors including substrate, bathymetry, tectonics, and hydrodynamics. Correlations between these physical factors and microbialite growth suggest that microbialites tend to grow on underlying raised substrate (Eardley, 1938; Chidsey and others, 2015; Bouton and others, 2016b; Bouton and others, 2016a; Vennin and others, 2019; Vanden Berg, 2019; Kanik and others, 2020; Baskin and others, 2022). At the mesoscale, the interior composition of the microbialites includes primarily clotted aragonite (posited to be of direct microbial origin (Pace et al, 2016; Vanden Berg, 2019), as well as trapped and cemented ooids, *Artemia* (brine shrimp) pellets, and some allochthonous grains (Chidsey and others, 2015). Many microbialites also include poorly-defined, laminated stromatolitic fabrics as a minor interior component. Thus, the term microbialite since the structures comprise a mix of fabric types, instead of using more specific terms such as stromatolite, thrombolite, or leolite.

Radiocarbon (^{14}C) dating of both solid carbonate and trapped organic material has yielded ages for microbialite material of 12.7–2.7 ka (Figure 1A) (Bouton and others, 2016b; Bouton and others, 2016a; Newell and others, 2017). The reservoir effect in the modern lake appears to be on the order of several hundred years (Bowen and others, 2019; Paradis and others, 2023), however, it may have been greater in the past (Bowen and others, 2019), and carbonate formation in close association with groundwater may incorporate a reservoir effect of over 5000 years (Homewood and others, 2022). Thus, there is a rather high degree of uncertainty in microbialite radiocarbon ages. Notwithstanding, to date, no modern ages have been measured from microbialite material, although dating is limited to only six microbialites from two locations at the northwest shore of Antelope Island, and none targeted periphyton-rich outer zones where modern carbonate precipitation appears to be happening (for example, Pace and others, 2016). It also appears that microbialites form over thousands of years, with a range from 7.6–12.7 cal ka measured from organic material extracted from four zones within a single microbialite (Newell and others, 2017). This covers a period when the surface elevation of Great Salt Lake is poorly constrained within a rough range of

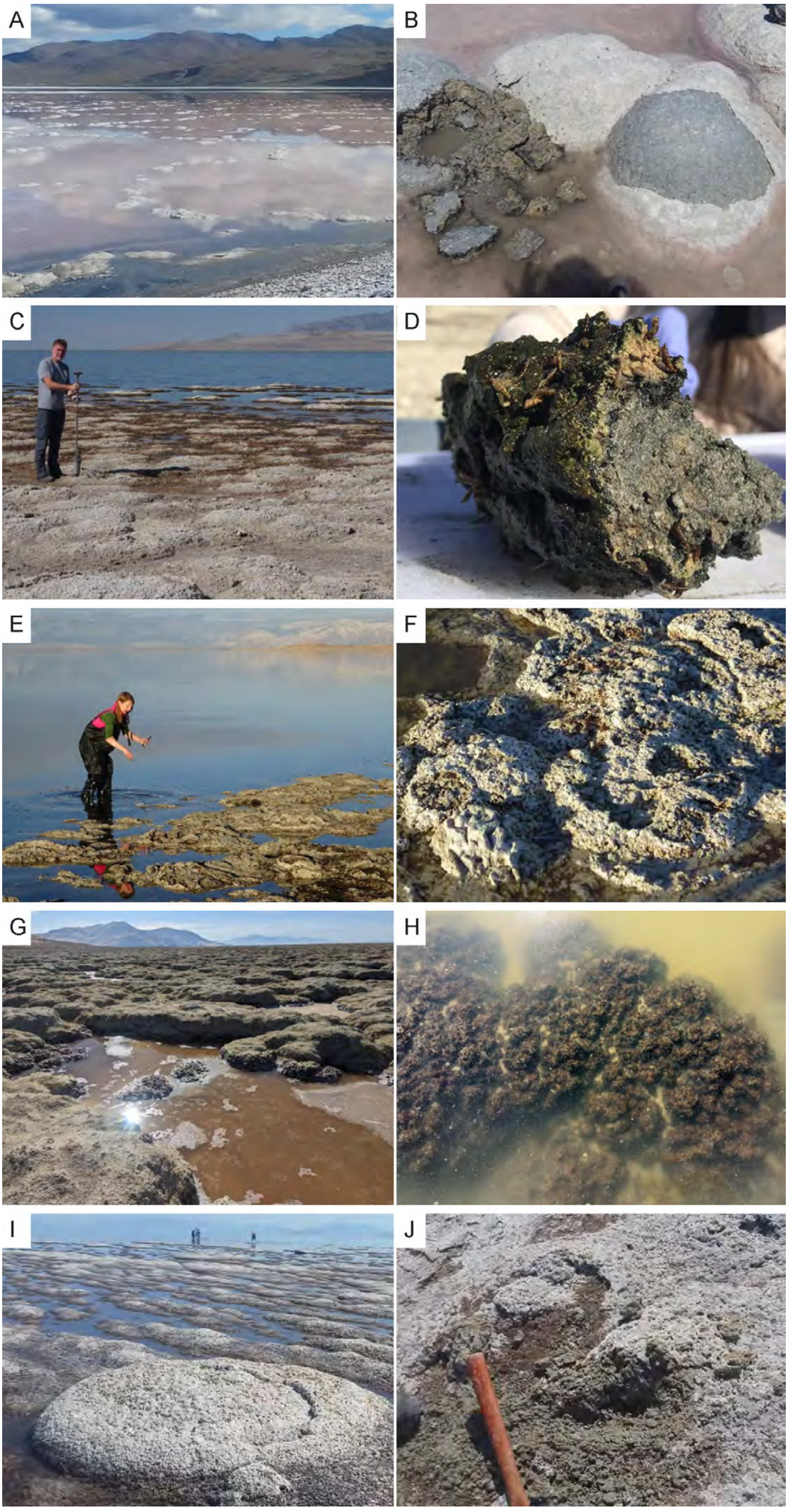

Figure 2. *Photographs of microbialites in and around Great Salt Lake. (A–B) Microbialites that grew at the boundaries of desiccation polygons at Promontory Point, north arm. Note the bright/light surface color (photosynthetic microbial mats are absent) of partially submerged microbialites in halite-saturated north arm water. (C–D) Microbialite reef at Ladyfinger Point on Antelope Island, showing transition from living periphyton to desiccated bright forms, (D) healthy mat and brine fly pupae visible on the surface of a collected microbialite sample; sample is roughly 14 cm across. (E–F) Microbialites at Bridger Bay off Antelope Island, showing (F) collapsed centers; area shown is roughly 1 m across. (G–H) Microbialite reef at Buffalo Point on Antelope Island, showing both exposed and partially-eroded structures, as well as (H) submerged structures with a dark, photosynthetic periphyton; area shown is roughly 0.8 m across. (I–J) Large and elongate microbialites off of Stansbury Island, with thrombolitic crust. Partially eroded crust visible in (J); area shown is roughly 1 m across. Locations where each set of photographs were taken are shown as markers on the map in Fig. 8.*

1271–1285 masl (4170–4216 ft-asl) (Oviatt and others, 2021) (Figure 1A).

Regardless of their age and origin, microbialites play an important role in the modern Great Salt Lake. The exposure of vast expanses of microbialites with historically low lake elevation levels is threatening their preservation and keystone function in the Great Salt Lake ecosystem. Great Salt Lake comprises distinct habitat types ranging from fresh– to brackish-water estuaries and wetlands where rivers enter the lake, to expansive mudflats and playas, to the hypersaline open water of Gunnison Bay (the north arm) and the south arm of Great Salt Lake. Great Salt Lake has historically supported a simple but hemispherically important ecosystem (Figure 3). Ten million birds rely on the lake, including 90% of the world's Eared Grebes (*Podiceps nigricollis*), two species of Phalaropes (*Phalaropus lobatus* and *Phalaropus tricolor*), and large nesting colonies of American White Pelicans (*Pelecanus erythrorhynchos*) and California Gulls (*Larus californicus*) (Conover and Bell, 2020). The lake also supports an economically important brine shrimp cyst-harvesting industry, which supports global aquaculture (Marden and others, 2020). Great Salt Lake's microbialites are a critical feature that supports this extreme ecosystem. Microbialites, the lithified structures, are distinct from microbialite periphyton communities, which, in Great Salt Lake, are robust, productive, and diverse microbial communities that blanket microbialite surfaces (Pace and others, 2016; Lindsay and others, 2017; Kanik and others, 2020; Ingalls and others, 2020). Microbialite periphyton communities are conservatively estimated to be responsible for 30% of the lake's primary productivity (Wurtsbaugh and others, 2011; Anderson and others, 2020; unpublished data by B. Baxter and others, 2023), the remainder is attributed to planktonic algae. The significance of microbialites is as anchored, solid substrates with substantial relief above the surrounding sediment in the Great Salt Lake benthos, providing islands of stability in otherwise mobile sediment where robust mats of photosynthetic microbes can develop. Microbialites can contribute biomass to pelagic zones via sloughing, wave action,

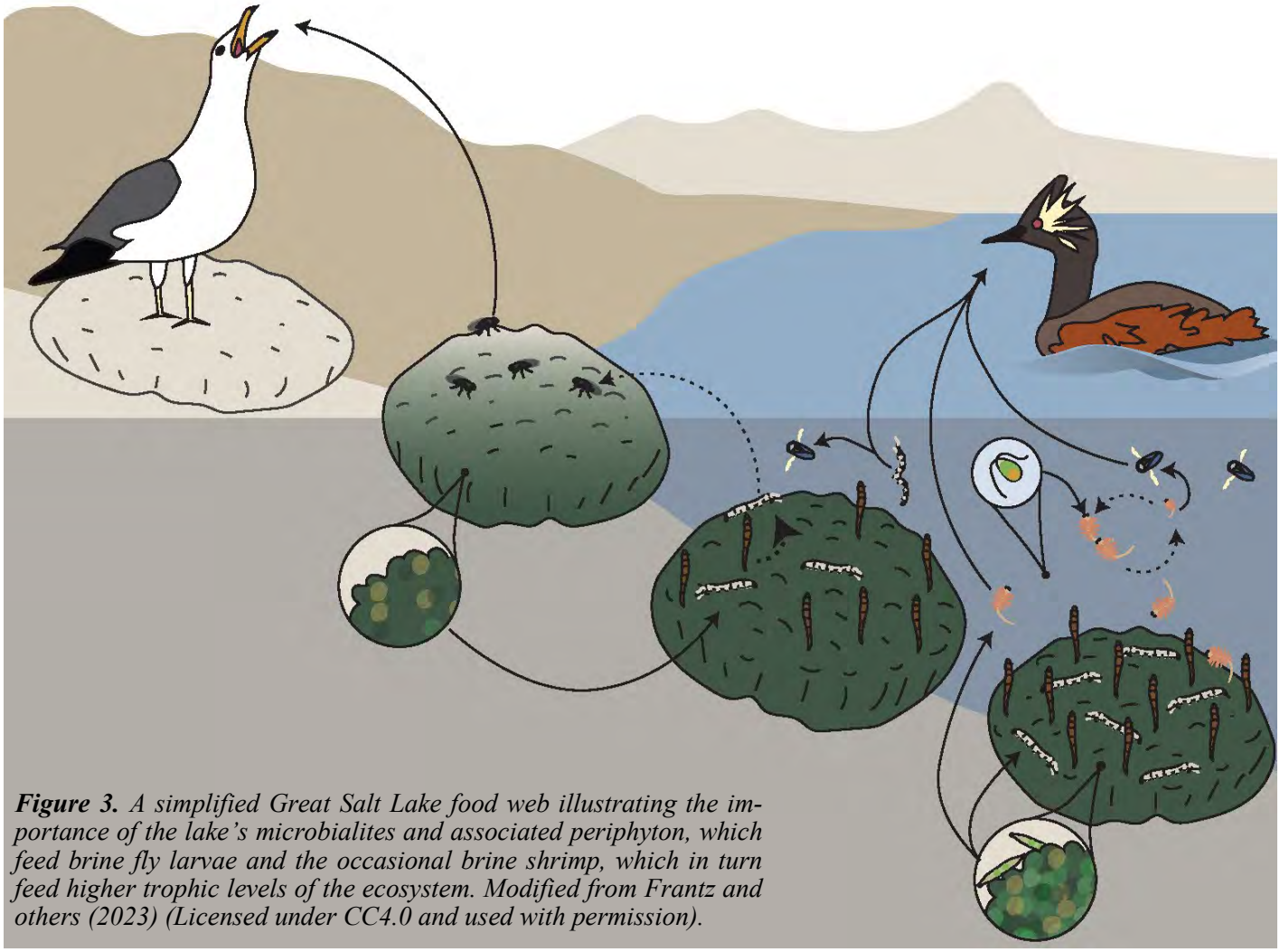

Figure 3. *A simplified Great Salt Lake food web illustrating the importance of the lake's microbialites and associated periphyton, which feed brine fly larvae and the occasional brine shrimp, which in turn feed higher trophic levels of the ecosystem. Modified from Frantz and others (2023) (Licensed under CC4.0 and used with permission).*

and/or bioturbation (MacIntyre and Melack, 1995; Barrett, 2020; Marden and others, 2020). Brine shrimp (*Artemia franciscana*) are filter feeders that prefer pelagic microalgae for nutrition, however, they will also graze on microbialite periphyton in shallow waters (Caudell and Conover, 2006; Lindsay and others, 2019; Brown and others, 2022). Indeed, stable isotope and gut content DNA evidence suggests that brine shrimp feed on microbialite surface communities during summer months (Barrett, 2020; Marden and others, 2020), presumably because the shrimp reduce the planktonic phytoplankton concentrations below the level at which they can efficiently feed (Belovsky and others, 2011), necessitating a supplementary food source.

Microbialites are also a critical part of the brine fly (*Ephydra* spp.) lifecycle, which depend on microbialites for habitat and food (Collins, 1980; Caudell and Conover, 2006; Belovsky and others, 2011; Wurtsbaugh and others, 2011; Conover and Bell, 2020; Brown and others, 2022), and are a critical nutritional source for both shorebirds and pelagic birds at Great Salt Lake (Conover and Bell, 2020; Sorensen and others, 2020). The overwhelming majority of brine flies appear to pupate on submerged microbialites (Collins, 1980; Wurtsbaugh, 2009), again, because they offer a stable benthic substrate. Hatched brine fly larvae then feed primarily on microbialite periphyton communities (Collins, 1980; Barrett, 2020). In shore areas where submerged microbialites are nearby and salinity levels do not exceed 20% (which may be an upper survival limit for microbialite primary producers; Lindsay and others, 2019), the dense clouds of hatched brine flies in late summer are remarkable; walking through a microbialite reef disturbs innumerable thousands of flies that rise from the surface of microbialites and ponded water in swarms.

Lake ecosystem models (for example, those described by Belovsky and others, 2011; Barrett, 2020) require accurate estimates of microbialite extent and relationships between lake elevation and the proportion of submerged vs. exposed microbialites.

Lake Level Fall and Exposure of the Lake's Microbialites

Great Salt Lake elevation levels have dropped to historic lows in recent years, the result of megadrought and overuse of water in the upstream watershed (Null and Wurtsbaugh, 2020), with profound consequences to the lake ecosystem. Avian nesting grounds that were previously protected from predation as islands have become connected to outer lake shores, disrupting bird populations (Kijowski and others, 2020; Sorensen and others, 2020). Increases in lake salinity have produced conditions that exceed levels at which keystone members of the ecosystem optimally survive and reproduce (Baxter and Butler, 2020; Great Salt Lake Salinity Advisory Committee, 2021). In addition, low elevation and consequent shoreline shift has exposed hundreds of kilometers of microbialite reefs, subjecting them—and their ecologically-important periphyton communities—to desiccation, negating their ecosystem function.

Recent work by Frantz and others (2023) provided some hope in the face of current mass microbialite exposure, showing that exposed and desiccated microbialites can regain some of their periphyton community in relatively short order once re-submerged in healthy lake water. However, their study was limited to a brief period of recovery, well before thick, carbonate-rich mats began to reappear (which could take years to decades). Their results also indicated that recovery is limited as lake level continues to fall and salinity continues to rise. In addition, they noted results that hint that individual microbialite areas harbor distinct strains of *Euhalothece*, the primary microbialite phototroph; losing areas of reef may therefore disrupt natural microbial diversity and could make the lake's microbialite-supported ecosystem less resilient to future change. Furthermore, they showed that subaerially exposed microbialites are rapidly weathered. Extended periods of exposure could reduce the height of microbialite reefs (and raise the surrounding sediment), diminishing their value as habitat for periphyton and brine fly larvae, even if lake levels rebound.

Mapping Great Salt Lake's Microbialites

The current threat to the lake's microbialites with lake level fall, and consequent long-term impacts on the lake ecosystem, mean that management of Great Salt Lake and its watershed requires a quantitative understanding of how different lake elevations affect microbialite exposure. This in turn depends on accurate maps of microbialite reef extent in Great Salt Lake, as well as refined relationships between lake bathymetry and microbialite exposure. Additionally, low lake levels and the exposure of the lake's microbialites has presented new hazards for navigation of watercraft on the lake. Accurate mapping of microbialite extent also has scientific value, as illustrated by several recent publications that have linked microbialite locations and extent to topographic features, faults, tectonics, wave energy, depth bands, and groundwater availability (Bouton and others, 2016b; Bouton and others, 2016a; Vanden Berg, 2019; Baskin and others, 2022).

The first map of microbialite extent was from Eardley (1938), who took advantage of a period of relatively low lake level in the mid-1930s to map them roughly from shore, as well as observing them at depths up to 1 m during "considerable travel" via a boat, the appropriately named *Hydrographer*, near the shores of the lake and in transects between the lake's islands. His paper includes both site and aerial photographs at various locations around the lake shore. Importantly, he also noted that cores from previously conducted engineering studies indicated prior periods of microbialite formation in the lake in areas different from where he had observed them. He used a planimeter and his map to determine a rough microbialite reef area of 398 km^2 (154 mi^2) within the lake (Figure 4). Due to limited mapping technology and limited field observations, Eardley's map largely missed microbialite reefs on the western side of the lake, as well as deeper-water areas, whereas extents on the east side of the north arm are overestimated. Overall, Eardley underestimated the extent of Great Salt Lake microbialites.

For his 2014 Ph.D. dissertation, Baskin (Baskin, 2014) produced the first major update to Eardley's map, utilizing single-beam sound-velocity soundings obtained during his work producing digital bathymetric surveys of the lake with the United States Geological Survey (USGS) (Baskin and Allen, 2005; Baskin and Turner, 2006). His method for identifying microbialites involved a calculation of rugosity from the sounding data that was truthed in select high-rugosity areas using dual-frequency 2D side scan sonar, swept-frequency Chirp sub bottom profiles, and videography (when lake visibility permitted), as well as *in situ* sampling in known microbialite locations. The extents identified in his dissertation were then updated and refined with the publication of Baskin and others (2022). This newer publication identified an area of ~1000 km^2 (~390 mi^2) of putative microbialite reef, with >700 km^2 (270 mi^2) in the south arm and >300 km^2 (~120 mi^2) in the north arm (Figure 4), nearly tripling the extent mapped by Eardley (1938). In his thesis, Baskin also noted the effect of the railroad causeway, completed in 1959, that bisected the lake and cut off the north arm from most of the lake's freshwater input, causing it to become rapidly salt-saturated and killing off the *Euhalothece*-based periphyton on north arm microbialites (this was also noted by Post, 1977, and verified with DNA sequencing by Lindsay and others, 2017). Although extensive, Baskin's map was largely based on indirect data; due to time and resource constraints he was only able to verify the presence of benthic microbialites in limited areas of his reported mapped extent.

Vanden Berg (2019) produced an alternative map of microbialite extent using Google Earth imagery and limited field mapping, yielding a microbialite reef aerial extent of 680 km^2. However, the map and extent estimates were limited by the availability of clear-water imagery and stated the need for further field verification.

Bouton and others (2020) further amended microbialite extent estimates by merging the Eardley (1938) and Baskin (2014) maps and adding additional refinement based on limited remote imagery of western Antelope Island from Bouton and others (2016a), yielding an expanded (and overestimated) microbialite reef aerial extent of 1261 km^2 (487 mi^2). In sum, maps of microbialite reef extent in the literature to date have given conflicting and highly variable results (Figure 4).

Recent low lake elevations and increasing resolution of satellite and aerial imagery have made microbialite mapping via remote imaging more powerful and accurate than ever before. Water column visibility in the lake varies greatly with season, biological activity, and weather, however, during clear-water periods the Secchi disk depth typically exceeds 3 m (10 ft), making the lake bottom visible from aerial view in all but the deepest portions of the lake (Belovsky and others, 2011). Microbialites are visible to depths in excess of 4 m (13 ft) in some high-visibility images, a fact that several studies have utilized to identify extents of microbialites against the lake bed (Bouton and others, 2016a; Vanden Berg, 2019). Advantages of using remote imagery over field-based mapping include the ability to quickly map large regions across the full extent of the lake (vs. transects or areas only accessible from shore), and that dry, shallow-water, and deep microbialites can all be mapped using the same method.

The varied estimates of microbialite extent from prior literature (Table 1) adds a large element of uncertainty to estimates of overall microbialite productivity, microbialite exposure, and other factors influencing the management of Great Salt Lake. Thus, our study attempted to improve on previous estimates by (1) mapping microbialites using satellite imagery, taking advantage of historic low lake level and improved spatial and temporal resolution of available images, (2) confirming (or refuting) the presence of suspected microbialite areas from prior mapping efforts via aerial imagery and field checks, and (3) generating shapefiles of microbialite reef extent that can be used in quantitative estimates of microbialite extent and exposure. Here, we present our results, which include the most detailed map of Great Salt Lake microbialite extent to date and a model of microbialite exposure at different lake elevations.

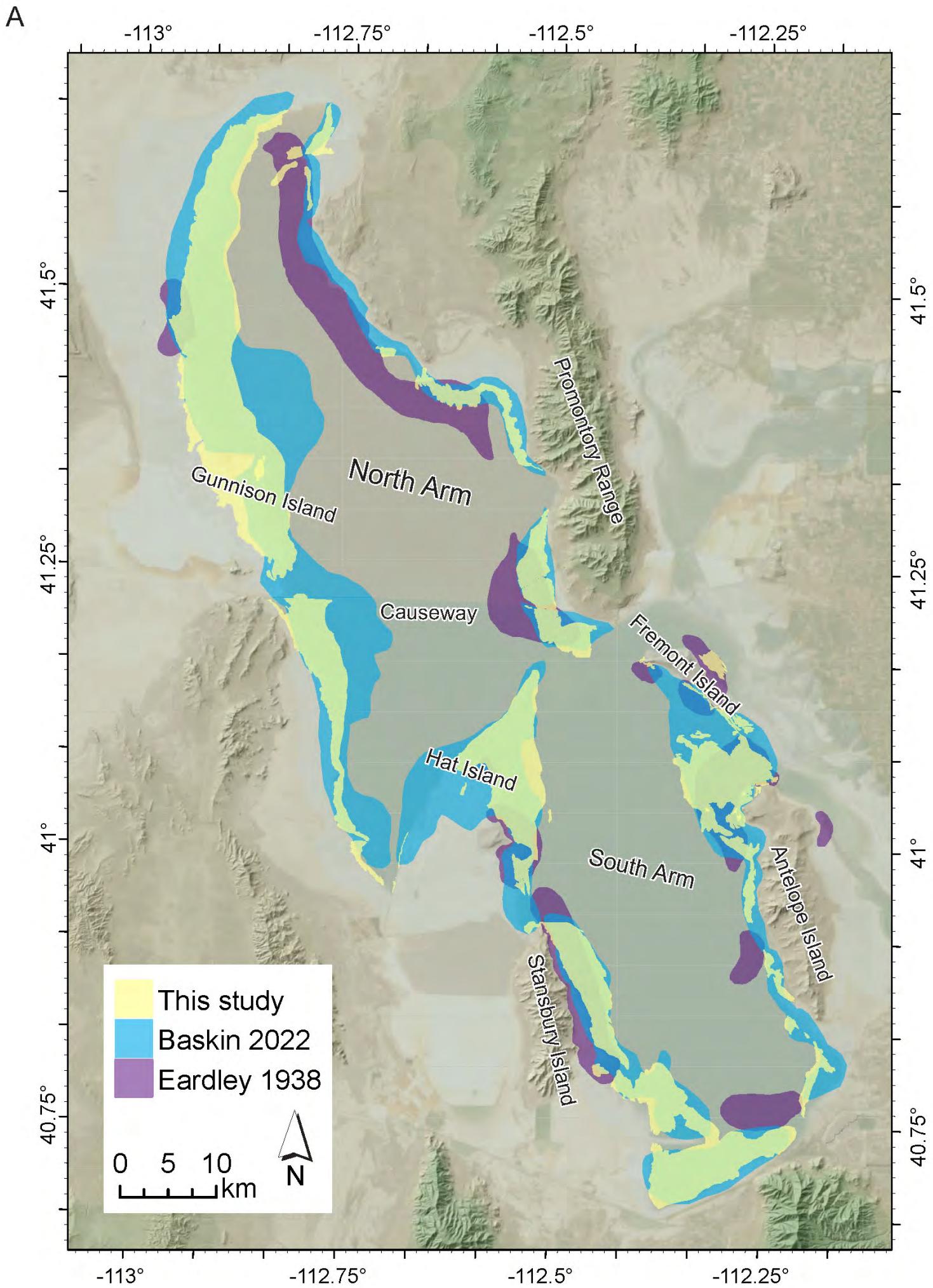

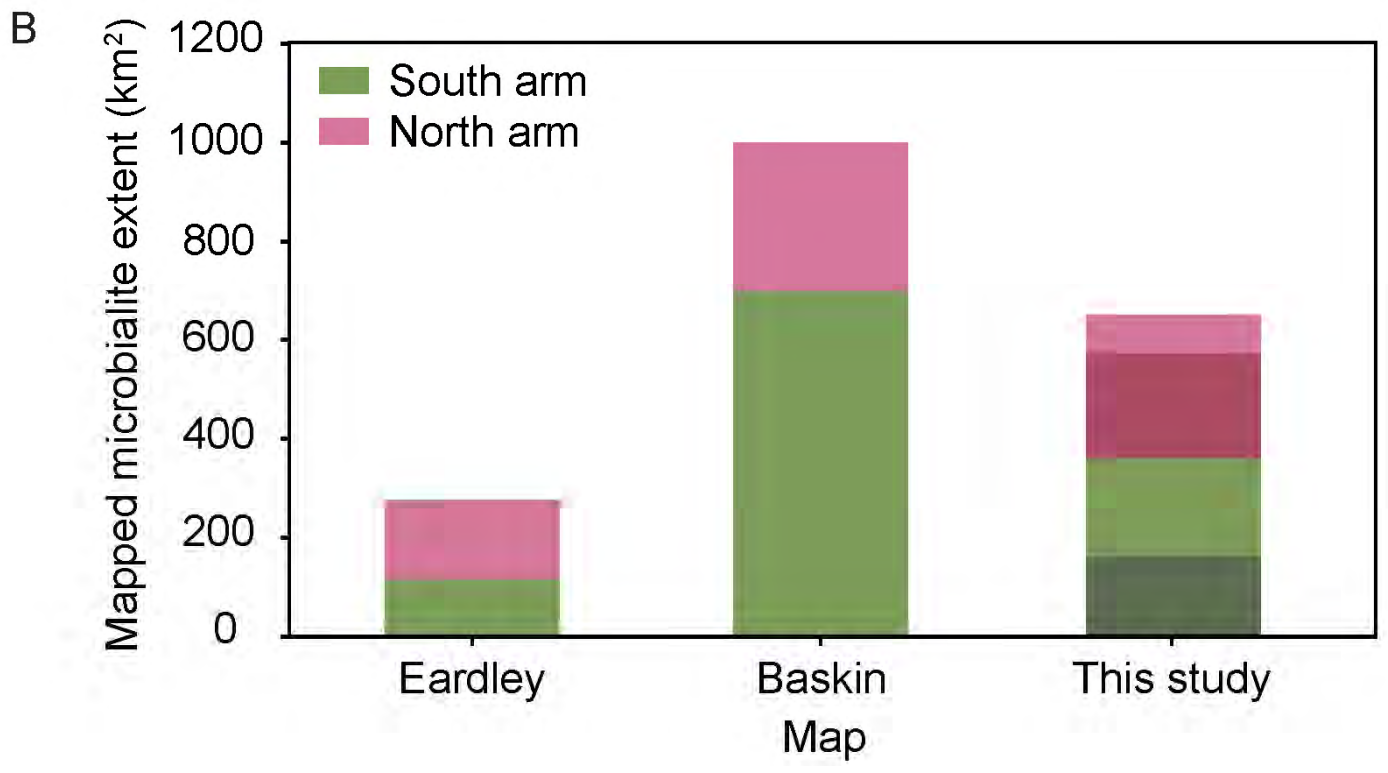

Figure 4. *Comparison of previously published microbialite reef extent maps for Great Salt Lake with our mapped reef extent. (A) Microbialite reef areas mapped by Eardley (1938; in purple), Baskin and others (2022; in blue), and this study (yellow), highlighting areas of overlap and major differences. (B) Quantified comparison of mapped reef areas in the three studies. Darker vs. lighter colors in the plot for this study indicate regions of high vs. low confidence.*

Table 1. *Summary of prior attempts to map lakebed microbialites in Great Salt Lake. Where given, reported values are non-italicized while values inferred from traced shapefiles are italicized.*

Reference	Method	Shortcomings and uncertainties	Mapped microbialite extent (km^2)		
			South Arm	North Arm	Total
Eardley, 1938	Field verification from shore and by boat	Limited to primarily nearshore areas confirmed in the field, missed areas of deeper microbialite reef and areas in the western portions of the lake	*117*	*160*	*277* 260
Baskin and others, 2022	Rugosity from acoustic soundings during bathymetric surveys, partially confirmed in the field	Indirect measure with limited field confirmation	700 *654*	300 *446*	1000 *1099*
Vanden Berg, 2019	Remote imagery	Limited image availability, limited field verification	*56*	*92*	*147*
Bouton and others, 2020	Merged prior maps with additional areas from remote imagery reported in Bouton and others, 2016a	Inherited uncertainties from prior work, assumed variable regions were due to burial vs. rip-up clasts			1261
This study (high confidence)	Remote imagery	Limited field verification, some deep-water areas could not be mapped	288	360	648

METHODS

Mapping Microbialites Using Satellite Imagery

Data Acquisition

Positive identification of microbialites through the application of remote sensing required high-resolution imagery with sufficient temporal resolution to permit analysis of areas of interest during favorable periods (i.e., periods without obscuring cloud cover, with low lake elevations, and with good water clarity). Imagery was collected through Esri's World Imagery Wayback (EWIW) archive. EWIW is a digital archive of published world imagery since 2014 that is stored as layer files that can be downloaded or viewed online through ArcGIS's living atlas. The current extent of the Great Salt Lake covers over 4000 km^2 within the Great Salt Lake basin (within the quad 40.6 –41.8°N, 111.8–113.2°W). Imagery for the region is collected via multiple satellite constellations at different temporal sequences that are location-dependent. North and south arms of Great Salt Lake required sets of time series imagery that often come from different capture dates (Table 2). EWIW acquires imagery via Landsat, USDA NAIP, TerraColor, Digital Globe, GeoEye IKONOS and AeroGRID at 0.6–15 m spatial resolution depending on location and provider.

Dates were selected to provide optimal below-water visibility, with favorable atmospheric conditions (especially low cloud cover), clear water periods (during the absence of water turbulence or algal blooms), and relatively low lake levels (permitting visibility in deeper areas of the lake), allowing good visual records of changing microbialite reef exposure (Figure 5). The analysis over multiple time points was vital for distinguishing loose debris from true reef, as illustrated in Figure 6. Google Earth Pro (GEP) was also utilized to compare and contrast visible reef zones with EWIW imagery. GEP utilizes Landsat and Copernicus satellite constellations for imagery collection. Dates of available archival GEP imagery vary; imagery from 2016–2022 provided the best clarity for positive or negative identification of microbialites. Imagery in GEP varies based on location and scale, with each view of lake locations utilizing several remote sensing sources and acquisition dates.

High-resolution historical imagery was collected from EWIW and downloaded as layer files. Once imported into ArcGIS Pro, each layer file was used for side-by-side comparison of microbialite structures. This side-by-side analysis of archived EWIW and GEP imagery was used to digitize areas that could be positively identified as reef zones via remote sensing.

Identification and Mapping

To develop criteria for microbialite reef identification, we first compared characteristics of known reef zones (from field studies by the authors) to our remote sensing imagery (Figure 7). We identified three reliable patterns for identifying microbialites in remote imagery.

Table 2. *Summary of remote imagery utilized for this study. Image Capture Date is the date satellite images were captured, while World Imagery Date is a date of availability in ArcGIS for the set of images.*

Image Capture Date	World Imagery Date	Location	Provider	Resolution (m)	Accuracy (m)
2014-06-29	2015-07-08	South Arm	NAIP	1	6
2014-08-31	2015-07-08	North Arm	NAIP	1	6
2016-06-26	2017-05-03	South Arm	NAIP	1	6
2016-07-15	2017-05-03	North Arm	NAIP	1	6
2016-05-07	2018-01-08	North Arm	Digital Globe	0.5	10.2
2013-08-29	2018-01-08	South Arm	Digital Globe	0.5	10.2
2022-05-07	2022-11-02	South Arm	Maxar (GEO1)	0.46	5
2021-10-15	2022-11-02	North Arm	Maxar (WV02)	0.5	5
2021-04-08	2022-12-14	South Arm	Maxar (GEO1)	0.46	5
2021-10-15	2022-12-14	North Arm	Maxar (WV02)	0.5	5

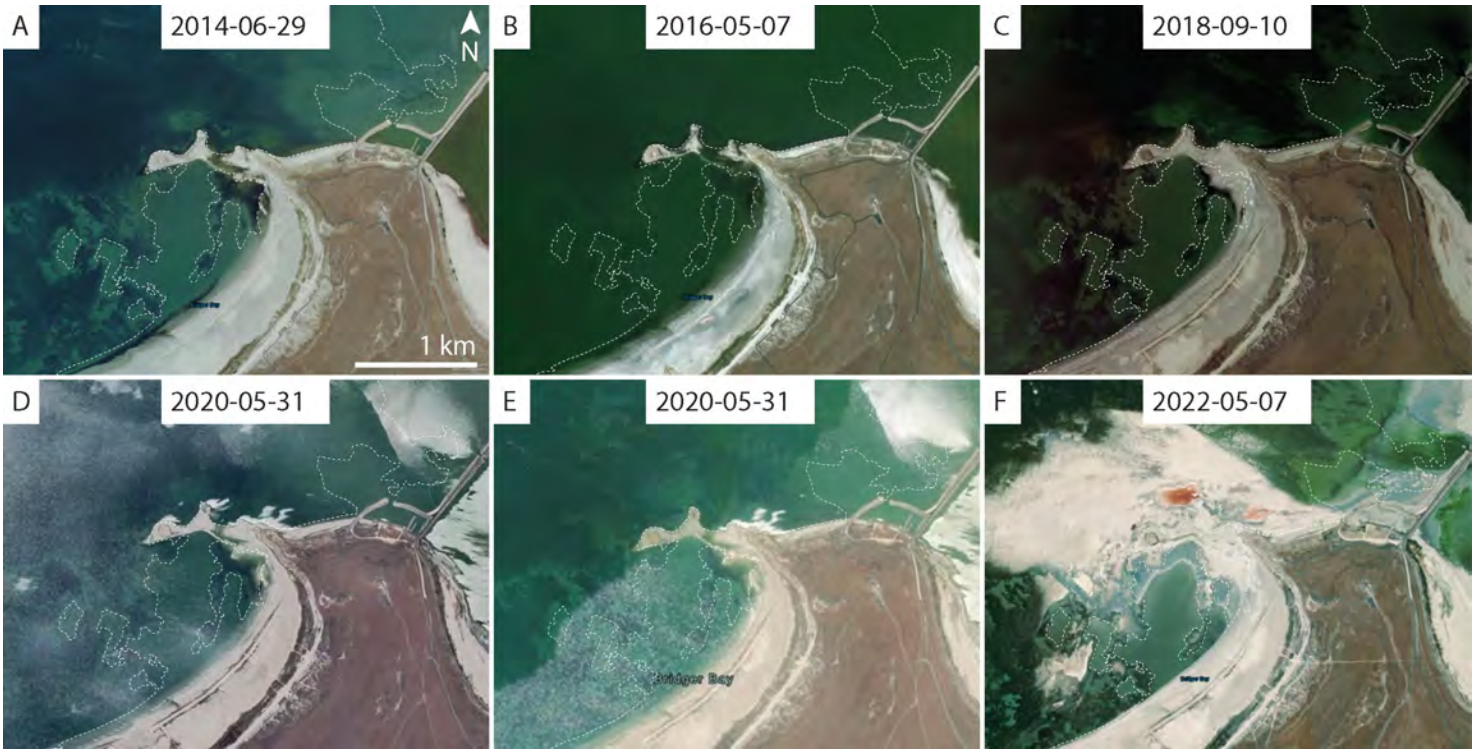

Figure 5. *Comparison of satellite images of a specific location at northern Antelope Island (41.06°, -112.26°) using different image dates. In all images, the thin, white dashed line shows the area outlined as microbialite reef in this study. (A) Microbialite reef can be seen as a dark green submerged region in June 2014 (Esri World Imagery Wayback). (B) In May 2016, visibility of the reef was limited due to poor water clarity and higher lake elevation (Esri World Imagery Wayback). (C) In September 2018, part of the visible reef was obscured due to image distortion and resolution issues (Google Earth Pro). (D) Waves on the lake in May 2020 obscure the reef (Google Earth Pro). (E) Waves and light reflection again obscure parts of the reef, with image stitching artifacts obscuring other portions (Esri World Imagery Wayback). (F) Exposed microbialite reef appear as bright/light regions during low lake level in May 2022 (Esri World Imagery Wayback).*

First, "healthy," submerged microbialites appear dark green in remote imagery and stand out against the brighter carbonate sediment background (Figs. 7A & 7D). In some instances of dark green submerged substrate, microbialite reefs were indistinguishable from loose microbialite debris (Figure 6) in single images; for such regions, we compared images from at least three different dates to look for evidence of mobility, with only stationary features mapped as reef.

Second, as lake levels fall, microbialites become exposed and "bleach" (Frantz and others, 2023), causing exposed reef areas to appear bright in partially-exposed reef areas. Our second identified pattern was that of white reef areas (bleached microbialites) with patterned high-relief mounds (for example, Figs. 7C & D).

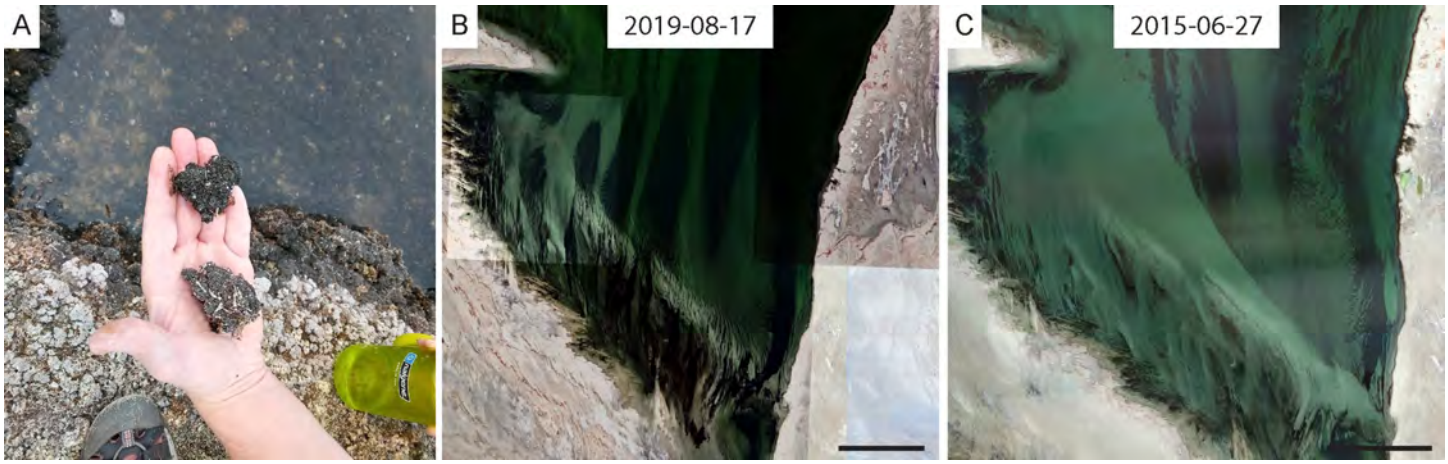

Figure 6. *Examples of mobile debris. (A) Field photograph of loose carbonaceous microbial mat debris between actual microbialite mounds at Buffalo Point in August 2021. (B) Google Earth Pro remote image showing a dark green region of potential microbialite reef in the southwest arm of the lake (40.983°, -112.709°) on 2019-08-17, and (C) Google Earth Pro remote image of the same location on 2015-06-27 showing shifted mobile debris. Scale bars in (B) and (C) are both 1 km.*

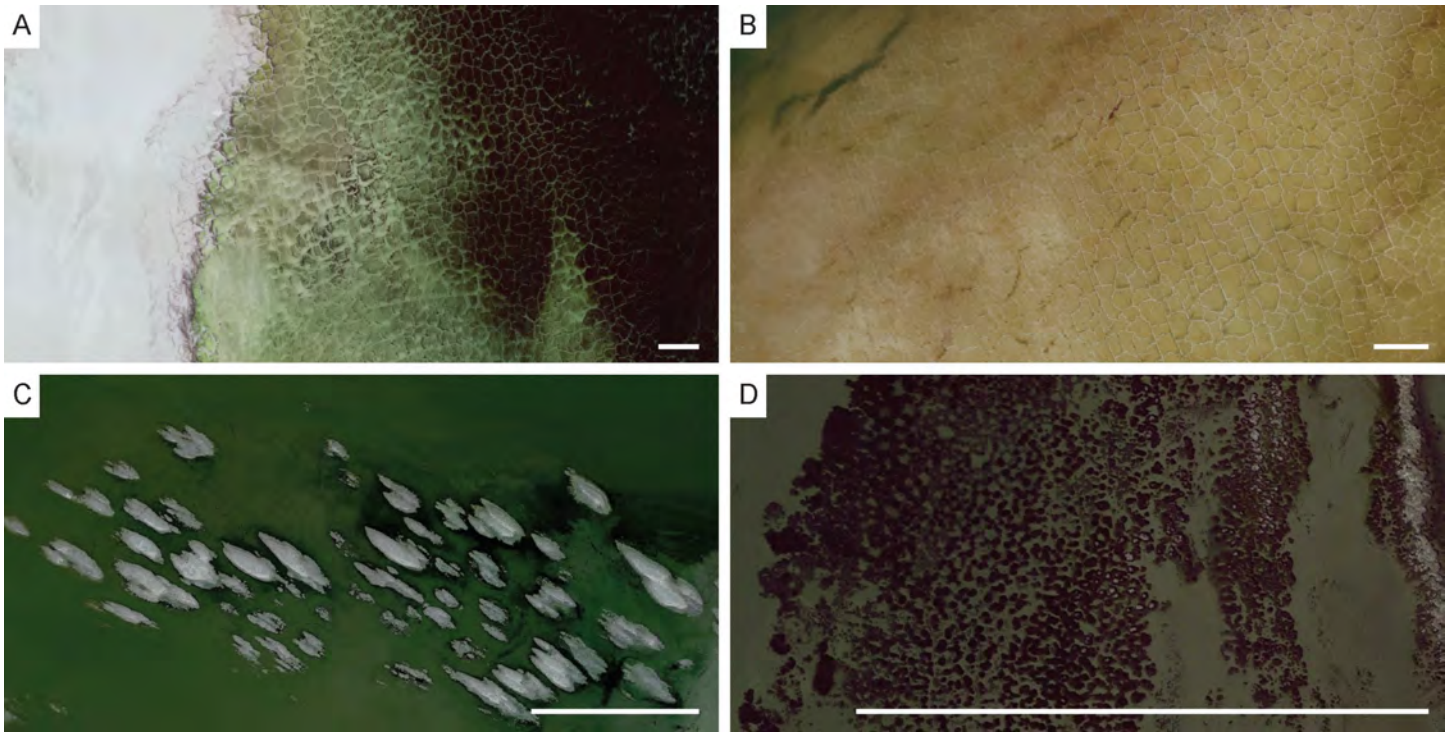

Figure 7. *Examples of field-verified microbialite reef areas identified from remote imagery in the south arm of Great Salt Lake. (A) Dark green submerged microbialites and bright bleached megapolygons indicate the presence of microbialites in a nearshore area in the south arm of the lake (41.073°, -112.573°). (B) Submerged desiccated microbialite-edged polygons in the north arm of the lake (41.249°, -112.533°). (C) Bright exposed and desiccated microbialites stand out against green lake water at a site near the Antelope Island marina (41.064°, -112.237°). (D) Partially submerged microbialites between Buffalo Point and White Rock Bay (41.033°, -112.275°). Scale bar in all images is 100 m. Image locations are shown as markers on the map in Fig. 8. Images from Google Earth Pro.*

Finally, microbialites tend to form on the perimeters of "megapolygons"—polygonal structures roughly 30–75 meters in diameter (Vanden Berg, 2019) (Figs. 7A & 7B). Thus, megapolygons are our third identified pattern. In contrast, zones of smaller desiccation–related polygons, averaging only 4–9 meters, are present along shoreline areas at higher elevation and are not associated with microbialites (Vanden Berg, 2019). These smaller polygons can be ephemeral, appearing and disappearing with changes in lake level.

In some areas, particularly north and northwest of Hat Island (112.586°W 41.071°N), we identified broad regions of megapolygons (some quite faint) at elevations above 4195 ft-asl, however, we excluded these from our map due to lack of field verification and their anomalously high elevations; if microbialites are found associated with these megapolygons, they might belong to an older generation.

Regions positively identified as containing micro-

bialite reefs were mapped in ESRI's ArcGIS Pro. Separate feature classes were created for the north and south arms and were digitized using ArcGIS Pro by tracing shapes over downloaded imagery. Feature classes as well as bathymetric layers were imported and projected as UTM NAD83 zone 12N to minimize distortion and maximize location accuracy. Areas were initially digitized in large zones before being refined to greater resolution in a second stage of processing.

Comparison to Prior Work

Areas mapped by prior studies were given extra attention in our analysis, with maps by Eardley (1938), Vanden Berg (2019), Bouton and others (2020), and Baskin and others (2022) providing a framework for the mapping efforts described in this study (Figure 4). Some regions identified as reef zones by Baskin and others (2022) were not able to be conclusively analyzed using remote imagery due to their occurrence in deeper areas of the lake. We included some of these regions from Baskin in our map as low-confidence regions.

Field Verification

Many identified reef sites were confirmed with field verification, particularly in accessible shoreline areas (Figure 8); these regions are denoted as high-confidence regions in our map. The western shores of the lake are difficult to access due in part to military restrictions and private land ownership, thus most sites on the west side of the lake have not been field verified. Identified reef sites not yet confirmed with field verification are denoted as low-confidence regions except for those associated with megapolygons, which were classified as high-confidence even in the absence of field verification.

Lake Elevation-Exposure Model

In order to develop a model of microbialite exposure at different lake elevations, we used shapefiles for the mapped microbialites and determined overlap with lake bathymetry shapefiles (1 ft intervals) imported from Baskin and Allen (2005) and Baskin and Turner (2006). However, caution should be exercised when using the historical bathymetry data, especially in the nearshore environment: modern observations during extreme low lake level indicate that these contours are significantly incorrect in several nearshore environments around the lake. Inaccuracies in the bathymetric data will create inaccuracies in the exposure models presented in this study, but currently this is the only published bathymetric data available. Microbialite reef area shapes were combined in distinct layers for the north vs. south arm of the lake, since the two arms can have independent water surface elevation levels and can be managed separately for ecosystem function. Digitized microbialite reef zones were split based on bathymetric data. These clipped zones were used to identify areas of exposure as lake levels decline.

Areas of mapped microbialite reef at elevations above bathymetric lines were considered exposed at that lake elevation, whereas areas of microbialite reef at or below bathymetric lines were considered submerged. The curve fit least-squares function in the scipy.optimize python package (Virtanen and others, 2020) was used to generate logistic regression models parameterized to fit the area vs. bathymetry elevation values for each arm of the lake using the least squares method.

RESULTS

Microbialite Reef Extent

Our remote imagery-based mapping of microbialite extent indicates 360 km^2 (139 mi^2) of microbialite reef between 1271.6 and 1280.5 masl (4172–4201 ft-asl) in the south arm of Great Salt Lake, of which 45% are high-confidence regions. In the north arm of the lake, we mapped 288 km^2 (111 mi^2) of microbialite reef in the same elevation band, of which 74% are high-confidence regions confirmed with field observation (Figure 8). The distributions of mapped microbialites by elevation were similar in the north and south arms (Figure S1), although our mapped region in the north arm was limited by limited field verification, poor water visibility, and image resolution.

Our mapped extent was somewhat similar with the Baskin and others (2022) map, with several important differences. First, we were able to map microbialites in exposed shore environments that were inaccessible by boat and therefore unable to be mapped sonographically by Baskin, thus, our map extends to higher elevations than the Baskin and others (2022) map (for example, bottom left of Figure 9C). Second, in some regions, areas mapped by Baskin extended deeper into the lake than what we found, for example, on the western shore of the lake (Figure 9B–C). Third, our map is more spatially refined (Figure 9E). Also, some regions mapped by Baskin were exposed as dry shoreline in recent years, with no apparent microbialites present (for example, Figure 9D).

Most (95%) of the microbialites that we mapped lie in an elevation band between 1274.0 and 1278.6

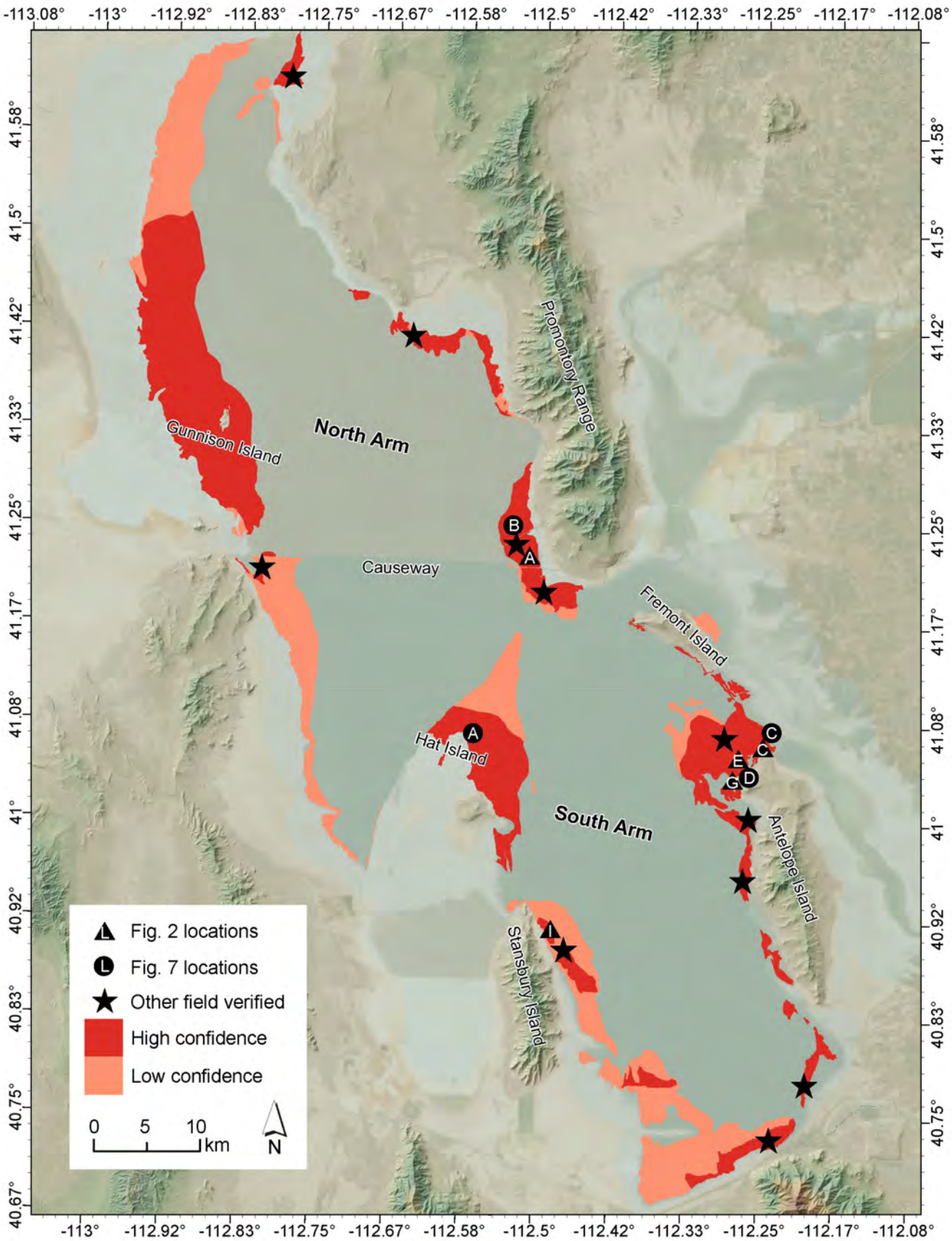

Figure 8. *Mapped extent of microbialites in Great Salt Lake (this study) showing regions of high confidence of microbialite occurrence (areas confirmed with field verification or presence of megapolygons) and regions mapped at low confidence of microbialite occurrence (areas of apparent microbialite reef in remote imagery). Stars indicate areas where field verification of microbialite reef existence (or non-existence) was verified. Triangles mark the approximate locations of photograph sets shown in Fig. 2. Circles mark the locations of remote imagery shown in Fig. 7. Basemap imagery provided by Earthstar Geographics.*

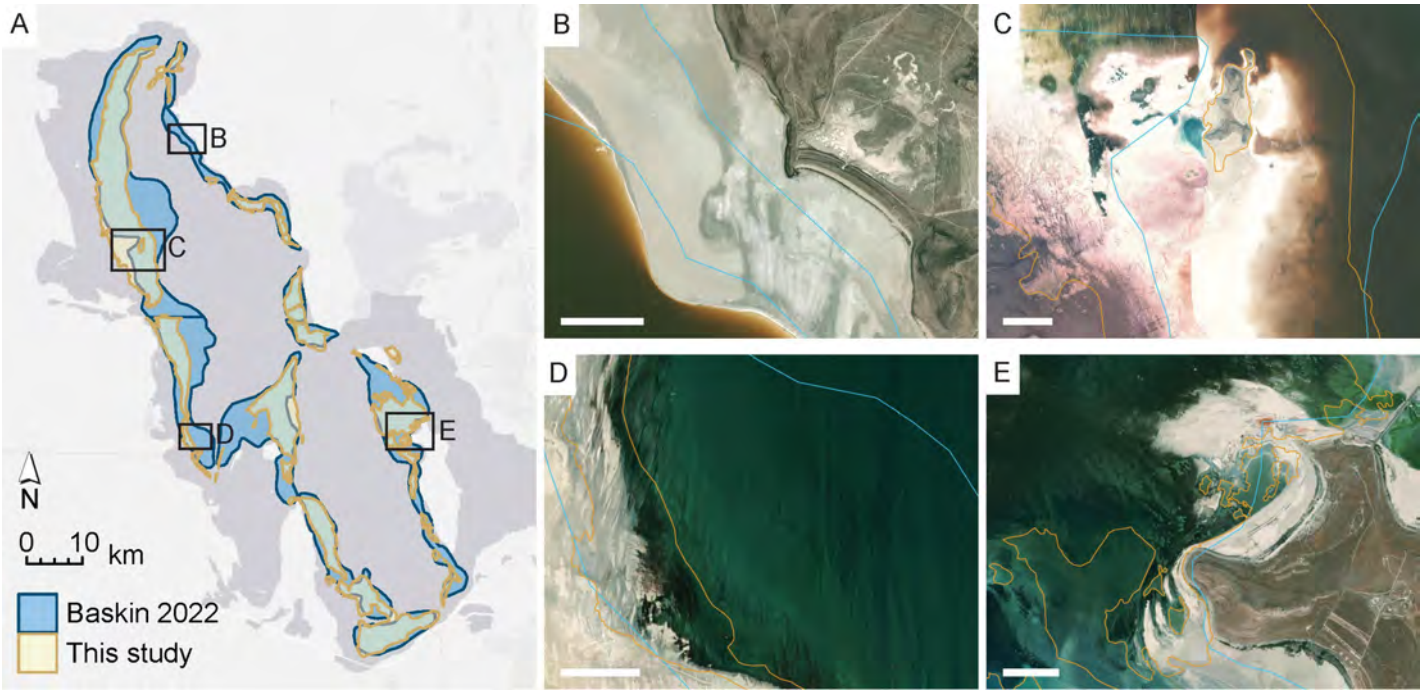

Figure 9. *Example detail areas where mapped microbialite extents in this study differed significantly from Baskin and others (2022). (A) Mapped microbialite extents in Baskin (blue) vs. this study (yellow) showing areas of detail (B–E). (B) Region along the northeastern lakeshore mapped as having microbialites by Baskin where we were unable to find evidence of microbialites in remote imagery or via field checks. Base image from Maxar 2015-07-08. (C) Area along the western shore of the lake where we identified a region of higher elevation microbialites visible in remote imagery but unmapped by Baskin. The Baskin map also extends into deeper water than we were able to confirm. Base image from Maxar 2015-04-27; mid-image color changes is an imagery artifact. (D) Area at the southwestern shore of the lake where the Baskin map includes microbialites where we only observed regions of mobile clasts. Base image from Maxar 2021-10-16. (E) Region off the northwest shore of Antelope Island where high-resolution imagery from Esri World Imagery Wayback and Google Earth Pro allowed for more precise mapping of microbialite reef zones in our study relative to the Baskin map. Base image from Maxar/Earthstar Geographics 2022-05-08. White scale bars in areas of detail (B–E) are all 1 km.*

masl (4180–4195 ft-asl) (Figure 10). Several notable deeper-water outlier areas are bounded by active Quaternary fault zones (Figure S2).

Elevation-Exposure Model

Our findings for microbialite exposure at different lake elevations are summarized in Table 3 and Figs. 11–12.

Fitting a logistic regression line (Equation 1) using the least-squares method to the lake elevation (*elev*, in masl or ft-asl) vs. microbialite exposure data (in km^2 or mi^2) gave r^2 values ≥ 0.995 for all models (Figure 12).

Equation 1: $$A_{exposed} = \frac{L}{1+e^{-k\cdot(x_0-elev)}} + b$$

In Equation 1, $A_{exposed}$ is the area (in km^2 or mi^2) of microbialites exposed at a given lake elevation (*elev*, in masl), where L, k, x_0, and b are model parameters defined in Table 4.

DISCUSSION

Refined Map of Microbialite Reef Extent for Great Salt Lake

Our remote imagery-based map of microbialite extent yielded an extent of microbialites between the lower and upper bounds of prior work (Figure 4): at both low and high confidence levels, we mapped significantly more microbialite area than Eardley (1938), but substantially less than what was mapped by Baskin and others (2022).

Because it relied on limited field observation and rough mapping tools available at the time, the Eardley (1938) map represents an understandable underestimate of microbialite extent. Meanwhile, the Baskin and others (2022) map covered the entire lakebed in relatively high resolution, however, by relying on indirect measurements of lake-bottom rugosity, it could have overestimated true microbialite extent. In general, our map refines the spatial extent of reefs identified by Baskin: 86% of our mapped regions were also mapped by Baskin, for both our high and low confi-

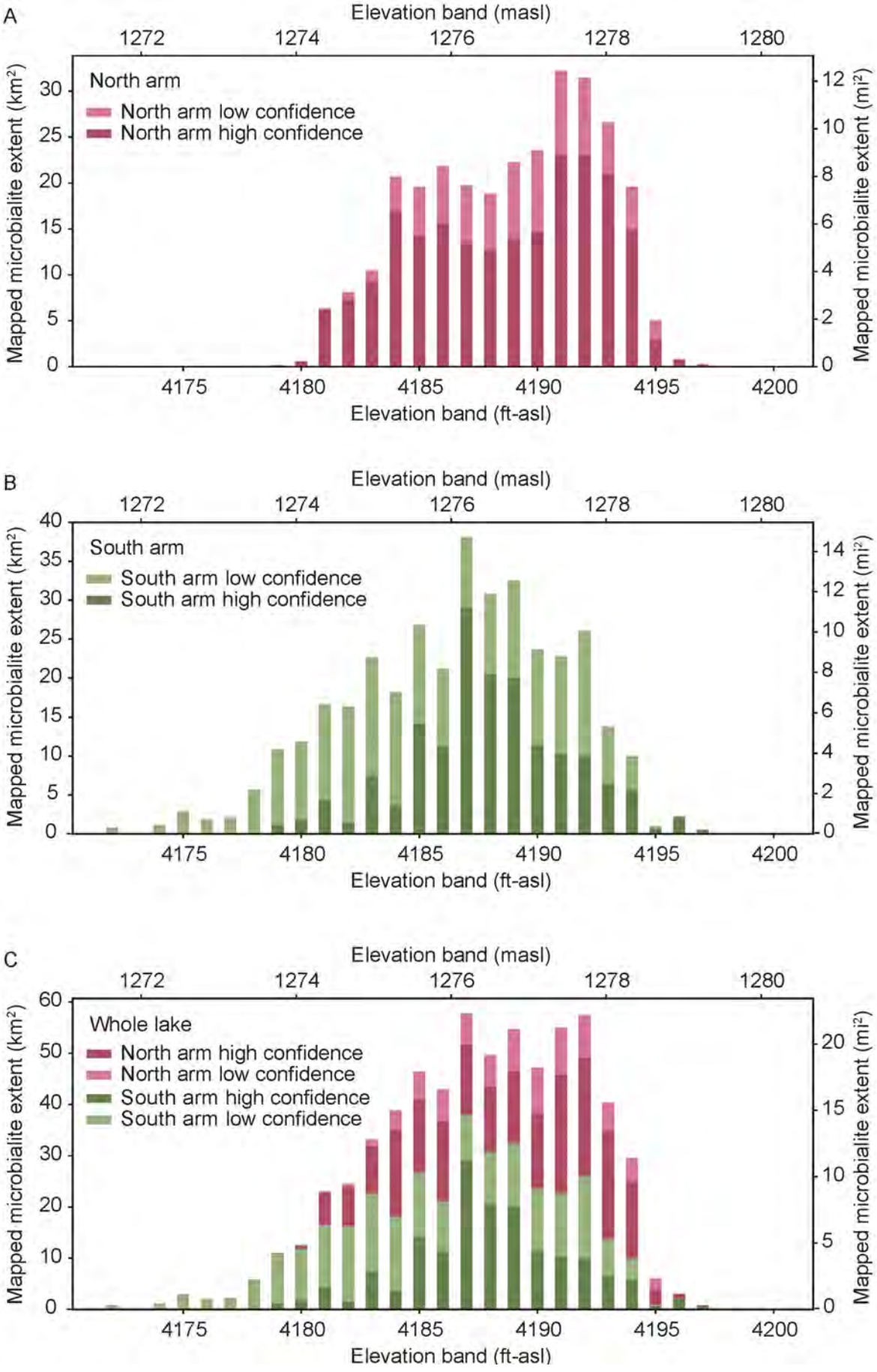

Figure 10. *Histograms of microbialite reef area identified at high and low confidence in different 1 ft elevation bands (labels show the lower bound of the band). (A) North arm (NA). (B) South arm (SA). (C) Both arms.*

Table 3. *Mapped microbialite reef area in different elevation bands, and area of microbialite exposure when lake level reaches the lower elevation bound.*

	Area of mapped microbialite reef (km2)				Total area exposed at lower elevation bound (km2)					
Elevation band	High confidence		Low confidence		High confidence		All mapped (high + low conf.)			
(ft-asl)	North Arm	South Arm	North Arm	South Arm	North Arm	South Arm	Whole lake	North Arm	South Arm	Whole lake
4172 – 4173	0.00	0.01	0.00	0.79	212.0	162.6	374.6	288.45	360.4	648.8
4173 – 4174	0.00	0.00	0.00	0.03	212.0	162.6	374.6	288.45	359.6	648.0
4174 – 4175	0.00	0.02	0.00	1.06	212.0	162.6	374.6	288.45	359.5	648.0
4175 – 4176	0.01	0.01	0.00	2.90	212.0	162.5	374.6	288.45	358.4	646.9
4176 – 4177	0.04	0.06	0.00	1.80	212.0	162.5	374.5	288.43	355.5	644.0
4177 – 4178	0.09	0.08	0.00	2.04	212.0	162.5	374.4	288.39	353.7	642.1
4178 – 4179	0.09	0.15	0.00	5.55	211.9	162.4	374.3	288.30	351.6	639.9
4179 – 4180	0.15	1.17	0.00	9.65	211.8	162.2	374.0	288.21	345.9	634.1
4180 – 4181	0.59	1.81	0.01	10.07	211.6	161.1	372.7	288.07	335.0	623.1
4181 – 4182	6.33	4.35	0.01	12.28	211.1	159.3	370.3	287.47	323.2	610.6
4182 – 4183	7.30	1.45	0.82	14.94	204.7	154.9	359.6	281.12	306.5	587.6
4183 – 4184	9.36	7.41	1.16	15.21	197.4	153.5	350.9	273.00	290.1	563.1
4184 – 4185	16.90	3.66	3.78	14.49	188.1	146.0	334.1	262.48	267.5	530.0
4185 – 4186	14.32	14.12	5.30	12.67	171.2	142.4	313.5	241.80	249.4	491.2
4186 – 4187	15.62	11.27	6.19	9.90	156.8	128.3	285.1	222.18	222.6	444.8
4187 – 4188	13.67	29.04	6.05	9.06	141.2	117.0	258.2	200.37	201.4	401.8
4188 – 4189	12.73	20.46	6.09	10.36	127.5	88.0	215.5	180.64	163.3	344.0
4189 – 4190	13.99	20.04	8.26	12.43	114.8	67.5	182.3	161.82	132.5	294.3
4190 – 4191	14.65	11.45	8.91	12.21	100.8	47.5	148.3	139.58	100.0	239.6
4191 – 4192	23.07	10.32	9.15	12.43	86.2	36.0	122.2	116.02	76.4	192.4
4192 – 4193	23.11	10.01	8.31	16.06	63.1	25.7	88.8	83.80	53.6	137.4
4193 – 4194	21.04	6.50	5.52	7.30	40.0	15.7	55.7	52.38	27.5	79.9
4194 – 4195	14.96	5.71	4.63	4.28	19.0	9.2	28.1	25.82	13.7	39.5
4195 – 4196	2.91	0.71	2.15	0.24	4.0	3.5	7.5	6.22	3.7	10.0
4196 – 4197	0.77	2.19	0.07	0.03	1.1	2.8	3.8	1.16	2.8	4.0
4197 – 4198	0.25	0.54	0.00	0.00	0.3	0.6	0.9	0.32	0.6	0.9
4198 – 4199	0.07	0.00	0.00	0.00	0.1	0.0	0.1	0.07	0.0	0.1
4199 – 4200	0.00	0.01	0.00	0.00	0.0	0.0	0.0	0.00	0.0	0.0
4200 – 4201	0.00	0.01	0.00	0.00	0.0	0.0	0.0	0.00	0.0	0.0

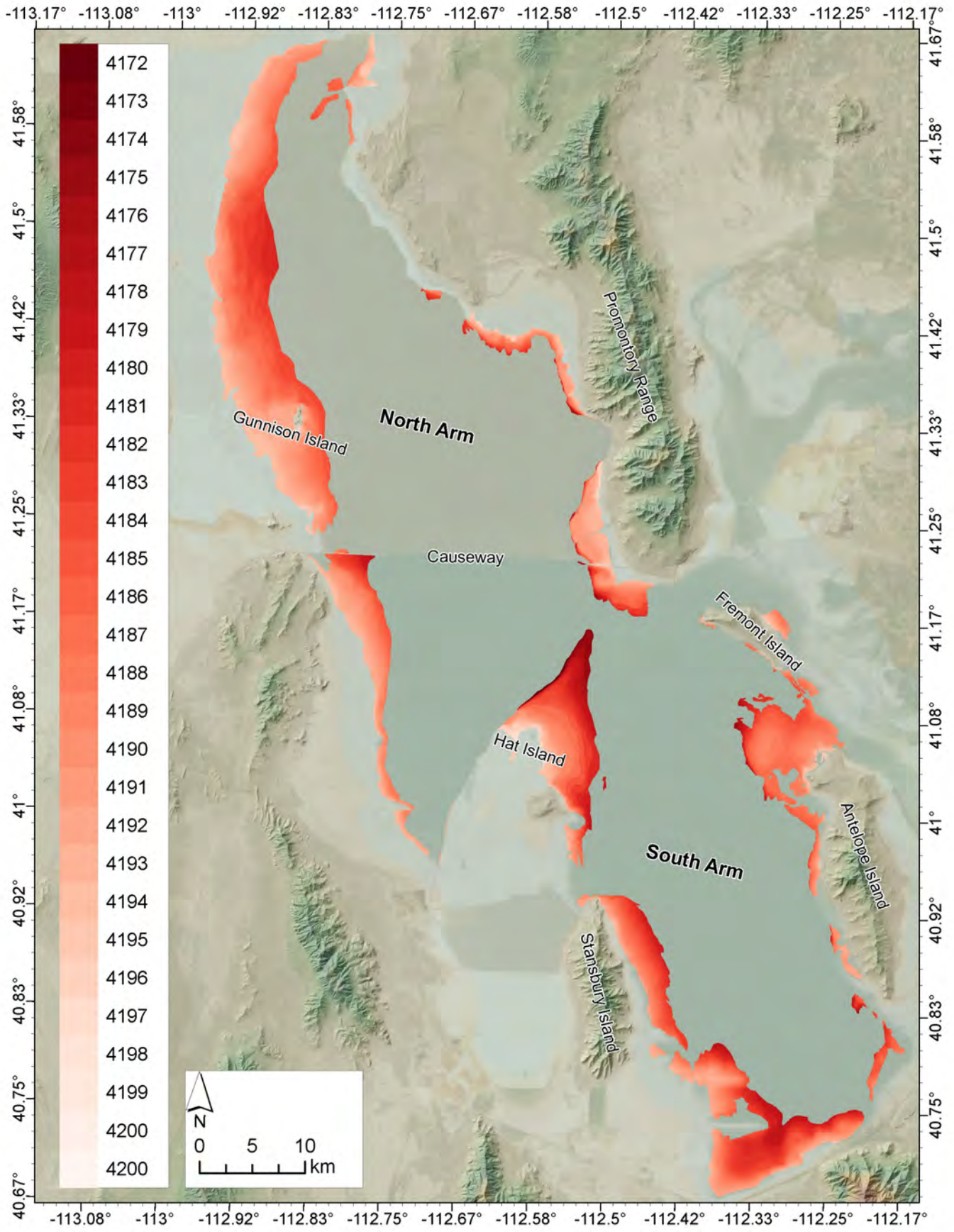

Figure 11. *Map of microbialite reef areas (this study) correlated with lake bathymetry, highlighting the areas of microbialite reef exposed at different lake surface elevations (in ft-asl). Basemap imagery provided by Earthstar Geographics.*

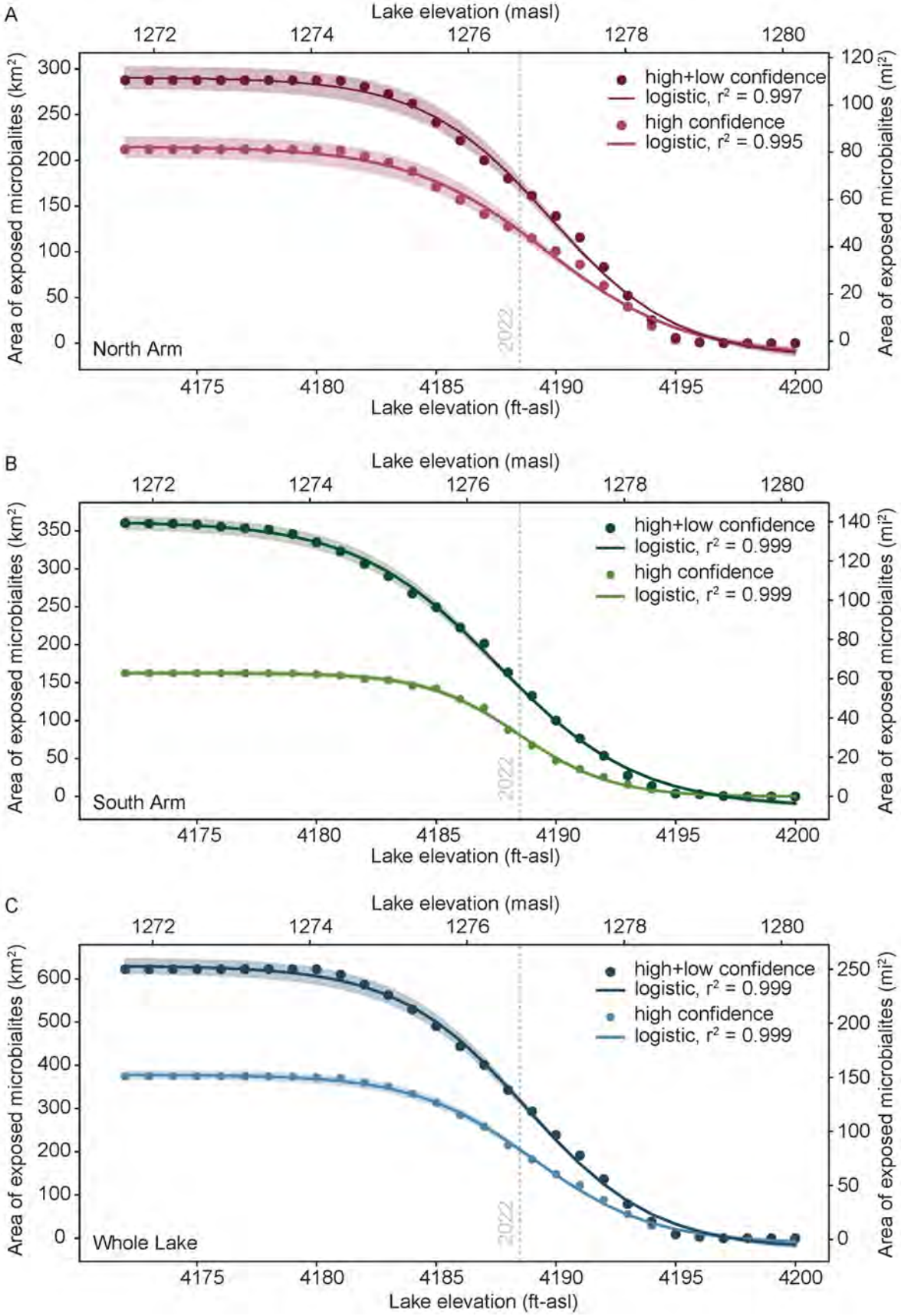

Figure 12. *Relationship between lake elevation and total cumulative microbialite exposure in Great Salt Lake. Data points for each elevation band that we mapped are shown as points along with corresponding logistic regression best-fit lines. Shaded areas represent the range of standard error for the regression models. The dashed vertical line marks the lake elevation at the autumn 2022 minimum (4188.5 ft-asl). (A) Microbialites mapped in the north arm of Great Salt Lake at high (light) and high+low (dark) confidence. (B) Microbialites mapped in the south arm of Great Salt Lake at high (light) and high+low (dark) confidence. (C) Values for the whole lake, with mapped microbialites at high (light) and high+low (dark) confidence.*

Table 4. *Logistic regression model results for microbialite exposure area at different lake elevations. To aid in the use of models for management, values are presented for use of both metric units (masl for lake elevation, km² for area of exposed microbialites) and imperial units (ft-asl for lake elevation, mi² for area of exposed microbialites).*

			Logistic regression model parameters - metric units (masl, km²)				**Logistic regression model parameters - imperial units** (ft-asl, mi²)			
Arm	**Confidence**	**r²**	**L**	**k**	**x_o**	**b**	**L**	**k**	**x_o**	**b**
North Arm	high	0.9954	229 ± 6	1.14 ± 0.07	1277.0 ± 0.1	-14 ± 5	88 ± 2	0.35 ± 0.02	4189.6 ± 0.2	-5.4 ± 1.8
North Arm	high+low	0.9967	308 ± 6	1.23 ± 0.06	1277.0 ± 0.1	-16 ± 5	119 ± 2	0.38 ± 0.02	4189.8 ± 0.2	-6.3 ± 1.9
South Arm	high	0.9992	163 ± 1	1.71 ± 0.04	1276.7 ± 0.0	0 ± 1	63 ± 0	0.52 ± 0.01	4188.5 ± 0.1	-0.1 ± 0.4
South Arm	high+low	0.9988	376 ± 5	1.12 ± 0.04	1276.4 ± 0.0	-14 ± 3	145 ± 2	0.34 ± 0.01	4187.5 ± 0.1	-5.5 ± 1.2
Whole lake	high	0.9988	390 ± 4	1.32 ± 0.04	1276.8 ± 0.0	-12 ± 3	151 ± 2	0.40 ± 0.01	4189.1 ± 0.1	-4.7 ± 1.3
Whole lake	high+low	0.9986	684 ± 9	1.14 ± 0.04	1276.7 ± 0.0	-31 ± 7	264 ± 4	0.35 ± 0.01	4188.6 ± 0.1	-12.0 ± 2.6

dence maps. However, Baskin mapped ~350 km² (135 mi²) more microbialite areas than we could confirm, largely in deep-water areas of the lake. There are several key differences between our map and the Baskin map that warrant future field verification. First, our technique allowed for mapping of microbialites in shore environments that were not navigable and therefore unmapped by Baskin, for example, in an area north of Lakeside where we identified desiccation megapolygons (Figure 9B). Second, areas mapped by Baskin frequently extended deeper into the lake than our remote imagery-based approach permitted, for example, on the western shore of the lake, and in the area between Antelope Island and Fremont Island (Figs. 4, 9B–C). We did not include these deeper-area regions of putative reef mapped by Baskin in our map or elevation-exposure model, however, we cannot rule out that they exist. Also, our map only accounts for consistently unburied microbialites, which are more likely to contribute to lake productivity than intermittently buried microbialites, which could have been included in the Baskin and others (2022) map. Heavily eroded microbialites may also have been missed by our map.

Lake Elevation and Microbialite Exposure

During the autumn 2022 historic lake lowstand of 1276.7 masl (4188.5 ft-asl), we estimate (from microbialites mapped at both high and low confidence in this study) that >294 km² (114 mi², or >45%) of the lake's microbialites were exposed, >133 km² (51 mi²) in the south arm (>37% exposure), and 162 km² (63 mi²) in the north arm (>56% exposure). Microbialites in the lake's north arm no longer support a robust microbialite surface community because of the arm's high salinity levels (Lindsay and others, 2019), thus, their exposure or submergence likely does not have much influence on the support of higher tropic levels in the Great Salt Lake food web. In the south arm, recent evidence suggests that microbialite photosynthetic (periphyton) communities can survive months of subaerial exposure, and that re-submerged microbialites appear to be rapidly recolonized by lake water microorganisms (Frantz and others, 2023). However, subaerially exposed microbialites cannot contribute to the benthic or planktonic food chains in the lake. Additionally, areas of microbialites that experienced frequent exposure in the past half century never fully redeveloped a healthy periphyton (marked by thick gelatinous mats) even when re-submerged for periods of several seasons to years, indicating that the damage caused by prolonged exposure is long-lasting. It is also important to note that microbialites in the hypersaline north arm of the lake also lack the robust mats of primary producers that are present in "healthy" microbialites (Lindsay and others, 2017); this is one of the reasons we clearly separate our maps of north vs. south arm microbialites. Finally, exposed microbialites are subjected to rapid weathering, and it could take decades or even centuries for the raised mounds that represent stable oases in an otherwise shifting lake benthos to re-form. Thus, the consequences of long-term subaerial exposure of the lake's microbialites are profoundly concerning for the lake ecosystem.

Even in the short term, there are ecosystem consequences of microbialite exposure. If microbialite periphyton communities conservatively represent 30% of primary production in Great Salt Lake, the expo-

sure of ~ 40% of them in the lake's south arm may have equated to a > 10% reduction in overall lake primary production in summer 2022 compared to "healthy" lake elevations (when microbialites are fully submerged). If one assumes that the bulk of microbialite-supported primary productivity occurs in relatively shallow water (i.e., the year-round photic zone), it is possible that the relative aerial extent of microbialites that occupy this zone has been relatively stable over the past several years of lake level fall, however, further lake level decline would substantially decrease the area of productive microbialites. Also significant to the ecosystem is the substantial decrease in *Ephydra* pupa anchor sites that occurs when microbialites become subaerially exposed.

The greatest change in submerged microbialites occurs between 1275.6 and 1278.0 masl (4185–4193 ft-asl; Figure 12) because of the large expanses and high density of microbialites in this zone (Figure 10). The lower bound for the lake elevation target range for management of 1279.5 masl (4198 ft-asl) (Utah DNR Forestry, 2013) ensures that nearly all of the lake's microbialites are submerged. At 1278 masl (4193 ft-asl), 88% are submerged, while at 1275.6 masl (4185 ft-asl), only 24% remain submerged. Additionally, at lake elevation levels below ~1277 masl (4190 ft-asl), microbialite community health becomes threatened not only by exposure, but by salinity. At salinity levels above 15%, the primary productivity of *Euhalothece*—and, thus, microbialite-associated productivity—declines (Lindsay and others, 2019); this corresponds to a lake elevation of roughly 1277 masl (4191 ft-asl). Thus, due both to microbialite exposure and high salinity levels, elevations above 1277 masl (4191 ft-asl) should be a minimum for lake management with respect to microbialite-supported ecosystem survival, whereas elevations above 1278.6 masl (4195 ft-asl) keep nearly all of the lake's microbialites submerged.

Limitations of this Study

Although we believe our map is a significant improvement over previously published maps of microbialite extent, it has several limitations and caveats.

First, our map is limited to visible reef areas. In regions where remote imagery is low resolution, we were unable to confidently map microbialites. We were also unable to conclusively confirm or refute microbialite reef areas in deep-water portions of the lake (generally, below 1275 masl, or 4183 ft-asl, although this varied somewhat by remote imagery available), where water obscures reflected light. These deep-water portions of the lake represent an area of 1800 km^2 (~700 mi^2) and include 232 km^2 (90 mi^2) of microbialite reef mapped by Baskin and others (2022); we cannot rule out the existence of microbialites above surrounding lake sediment at depths below 1275 masl (4183 ft-asl), but we were only able to confirm the probable existence of microbialites in 53 km^2 (20 mi^2) of that area based on remote imagery and the methods of our study. This could account for some, but not all discrepancies between the Baskin map and ours. This caveat to our study could be remedied with a comprehensive field verification campaign. Deep-water areas may need to be verified by divers. Our study could also be used to help refine Baskin's benthic rugosity-based mapping algorithm (Baskin, 2005).

Second, we excluded regions of reef that were not consistently visible in remote imagery. We did this to exclude areas of shifting microbialite debris/rip-up clasts. However, the change in visibility could also be due to shifting ooid sands covering up and then re-exposing areas of active reef (as noted by Bouton and others, 2016). These regions of reef could still, when exposed, contribute to primary production in the lake. Roughly 59 km^2 (23 mi^2) of the lakebed we analyzed in this study comprised regions of variable brightness, i.e., either mobile clasts or varied exposure/covering by surrounding sediment, and it was not possible to distinguish mobile clasts from shifting sediment obscuring true reef areas.

Third, our model of microbialite exposure vs. lake elevation is based on the bathymetry of Baskin and Allen (2005) and Baskin and Turner (2006), which was limited spatially to 1-km transects in the navigable portions of the lake (Baskin, 2005; Baskin, 2006). Thus, the bathymetry, especially in the elevation band of 1276.5–1278.6 masl (4188–4195 ft-asl), which corresponds to one of the greatest expanses of microbialite reef (Figure 10), is poorly constrained, limiting the accuracy of our model. Bathymetry in this band can be improved with detailed lidar mapping, work that is currently being explored and, we hope, done more extensively in the near future.

Finally, prolonged subaerial exposure of the lake's microbialites results in their rapid weathering (Frantz and others, 2023), thus, microbialite extents at higher elevation bands are subject to change (decrease) during periods of low lake elevation. Additional research is required to quantify and model rates of microbialite weathering.

SUMMARY

We mapped 649 km^2 (251 mi^2) of microbialite reef in Great Salt Lake by leveraging low lake levels and recent availability of high-resolution remote imagery. Of that, 375 km^2 (145 mi^2) were either field-

verified or were identified as megapolygons, which are linked to microbialites in Great Salt Lake (Vanden Berg, 2019). We believe that our map of microbialite extents refines previously published maps. We have also produced shapefiles of microbialite extent at different lake elevations (Supplemental Materials). Our model of microbialite exposure vs. lake elevation can be used to inform Great Salt Lake management: 1278.6 masl (4195 ft-asl) should be considered as a critical minimum lake elevation (with the understanding that higher lake levels provide greater protection) with respect to microbialites; at this depth, 98% of the lake's microbialites are submerged. During the historic lowstand in autumn 2022 of 1276.7 masl (4188.5 ft -asl), we estimate that >37% of the microbialites in the south arm of the lake were subaerially exposed, representing substantial damage to benthic primary productivity (which was likely already threatened by high salinity levels) and *Ephydra* larva habitat.

ACKNOWLEDGEMENTS

LW was supported by NSF RISE #1801760 to Elizabeth Balgord. CF was supported by NSF EAR #1826869. MVB was supported by the Utah Geological Survey.

We thank Ryan Frazier and Michael Hernandez for their extensive help with GIS aspects of this project, and several reviewers for detailed and helpful comments on a prior version of this manuscript.

REFERENCES

Anderson, N.L., Barrett, K.L., Jones, S.E., and Belovsky, G.E., 2020, Impact of abiotic factors on microbialite growth (Great Salt Lake, Utah, USA): a tank experiment: Hydrobiologia, v. 847, no. 9, p. 2113–2122, doi: 10.1007/s10750-020-04235-9.

Barrett, K.L., 2020, Microbialite communities and food web linkages in Great Salt Lake: Notre Dame, University of Notre Dame, Ph.D. Dissertation, 195 p.

Baskin, R., 2005, Calculation of area and volume for the south part of Great Salt Lake, Utah: USGS Open-File Report 2005–1327, 7 p.

Baskin, R.L., 2006, Calculation of area and volume for the north part of Great Salt Lake, Utah: USGS Open-File Report 2006–1359, 6 p.

Baskin, R.L., 2014, Occurrence and Spatial Distribution of Microbial Bioherms in Great Salt Lake, Utah: Salt Lake City, University of Utah, Ph.D. Dissertation, 203 p.

Baskin, R.L., and Allen, D.V., 2005, Bathymetric map of the south part of Great Salt Lake, Utah, 2005: U.S. Geological Survey Scientific Investigations map 2894, scale 1:24,000.

Baskin, R.L., Della Porta, G., and Wright, V.P., 2022, Characteristics and controls on the distribution of sublittoral microbial bioherms in Great Salt Lake, Utah: Implications for understanding microbialite development: The Depositional Record, v. 8, no. 1, p. 39–66, doi: 10.1002/dep2.159.

Baskin, R.L., and Turner, J., 2006, Bathymetric Map of the North Part of Great Salt Lake, Utah, 2006: U.S. Geological Survey Scientific Investigations Map 2954, scale 1:24,000.

Baxter, B.K., and Butler, J.K. (Eds.), 2020, Great Salt Lake Biology: A Terminal Lake in a Time of Change: Cham, Springer International Publishing, 527 p., doi: 10.1007/978-3-030-40352-2.

Belovsky, G.E., Stephens, D., Perschon, C., Birdsey, P., Paul, D., Naftz, D., Baskin, R., Larson, C., Mellison, C., Luft, J., Mosley, R., Mahon, H., Van Leeuwen, J., and Allen, D.V., 2011, The Great Salt Lake Ecosystem (Utah, USA): long term data and a structural equation approach: Ecosphere, v. 2, no. 3, p. 1–40, doi: 10.1890/ES10-00091.1.

Bouton, A., Vennin, E., Amiotte-Suchet, P., Thomazo, C., Sizun, J., Virgone, A., Gaucher, E.C., and Visscher, P.T., 2020, Prediction of the calcium carbonate budget in a sedimentary basin: A "source-to-sink" approach applied to Great Salt Lake, Utah, USA: Basin Research, v. 32, no. 5, p. 1005–1034, doi: 10.1111/bre.12412.

Bouton, A., Vennin, E., Boulle, J., Pace, A., Bourillot, R., Thomazo, C., Brayard, A., Désaubliaux, G., Goslar, T., Yokoyama, Y., Dupraz, C., and Visscher, P.T., 2016a, Linking the distribution of microbial deposits from the Great Salt Lake (Utah, USA) to tectonic and climatic processes: Biogeosciences, v. 13, p. 5511–5526, doi: 10.5194/bg-13-5511-2016.

Bouton, A., Vennin, E., Mulder, T., Pace, A., Bourillot, R., Thomazo, C., Brayard, A., Goslar, T., Buoncristiani, J.-F., Désaubliaux, G., and Visscher, P.T., 2016b, Enhanced development of lacustrine microbialites on gravity flow deposits, Great Salt Lake, Utah, USA: Sedimentary Geology, v. 341, p. 1–12, doi: 10.1016/j.sedgeo.2016.05.004.

Bowen, G.J., Nielson, K.E., and Eglinton, T.I., 2019, Multi-Substrate Radiocarbon Data Constrain Detrital and Reservoir Effects in Holocene Sediments of the Great Salt Lake, Utah: Radiocarbon, v. 61, no. 4, p. 905–926, doi: 10.1017/RDC.2019.62.

Brown, P.D., Craine, J.M., Richards, D., Chapman, A., and Marden, B., 2022, DNA metabarcoding of the phytoplankton of Great Salt Lake's Gilbert

Bay: Spatiotemporal assemblage changes and comparisons to microscopy: Journal of Great Lakes Research, v. 48, no. 1, p. 110–124, doi: 10.1016/j.jglr.2021.10.016.

Burne, R.V., and Moore, L.S., 1987, Microbialites: Organosedimentary Deposits of Benthic Microbial Communities: PALAIOS, v. 2, no. 3, p. 241–254., doi: 10.2307/3514674.

Carozzi, A.V., 1962, Observations on Algal Biostromes in the Great Salt Lake, Utah: The Journal of Geology, v. 70, no. 2, p. 246–252, doi: 10.1086/626814.

Caudell, J.N., and Conover, M.R., 2006, Energy content and digestibility of brine shrimp (*Artemia franciscana*) and other prey items of eared grebes (*Podiceps nigricollis*) on the Great Salt Lake, Utah: Biological Conservation, v. 130, no. 2, p. 251–254, doi: 10.1016/j.biocon.2005.12.018.

Chidsey, T.C., Vanden Berg, M.D., and Eby, D.E., 2015, Petrography and characterization of microbial carbonates and associated facies from modern Great Salt Lake and Uinta Basin's Eocene Green River Formation in Utah, USA: Geological Society, London, Special Publications, v. 418, no. 1, p. 261–286, doi: 10.1144/SP418.6.

Collins, N., 1980, Population ecology of Ephydra cinerea Jones (Diptera: Ephydridae), the only benthic metazoan of the Great Salt Lake, U.S.A.: Hydrobiologia, v. 68, no. 2, p. 99–112, doi: 10.1007/BF00019696.

Conover, M.R., and Bell, M.E., 2020, Importance of Great Salt Lake to Pelagic Birds: Eared Grebes, Phalaropes, Gulls, Ducks, and White Pelicans, *in* Baxter, B.K., and Butler, J.K., editors, Great Salt Lake Biology: A Terminal Lake in a Time of Change: Cham, Springer International Publishing, p. 239–262, doi: 10.1007/978-3-030-40352-2_8.

Cumings, E.R., and Shrock, R.R., 1928, Niagaran Coral Reefs of Indiana and Adjacent States and Their Stratigraphic Relations: GSA Bulletin, v. 39, no. 2, p. 579–620, doi: 10.1130/GSAB-39-579.

Domagalski, J.L., Orem, W.H., and Eugster, H.P., 1989, Organic geochemistry and brine composition in Great Salt, Mono, and Walker Lakes: Geochimica et Cosmochimica Acta, v. 53, no. 11, p. 2857–2872.

Dupraz, C., Reid, R.P., Braissant, O., Decho, A.W., Norman, R.S., and Visscher, P.T., 2009, Processes of carbonate precipitation in modern microbial mats: Earth-Science Reviews, v. 96, no. 3, p. 141–162, doi: 10.1016/j.earscirev.2008.10.005.

Eardley, A.J., 1938, Sediments of Great Salt Lake, Utah: AAPG Bulletin, v. 22, no. 10, p. 1305–1411.

Frantz, C.M., Gibby, C., Nilson, R., Stern, C.J., Nguyen, M., Ellsworth, C., Dolan, H., Sihapanya, A., Aeschlimann, J., and Baxter, B.K., 2023, Desiccation of ecosystem-critical microbialites in the shrinking Great Salt Lake, Utah (USA): PLOS Water, v. 2, no. 9, e1000100, doi: 10.1371/journal.pwat.0000100.

Frantz, C.M., Petryshyn, V.A., and Corsetti, F.A., 2015, Grain trapping by filamentous cyanobacterial and algal mats: implications for stromatolite microfabrics through time: Geobiology, v. 13, no. 5, p. 409–423, doi: 10.1111/gbi.12145.

Great Salt Lake Salinity Advisory Committee, 2021, Great Salt Lake Salinity Matrix 2021: Utah Division of Forestry, Fire & State Lands, 1 p.

Halley, R.B., 1976, Textural variation within Great Salt Lake algal mounds, *in* Walter, M.R., editor, Stromatolites: Elsevier Developments in Sedimentology, p. 435–445.

Hart, I., Jones, K.B., Brunelle, A., DeGraffenried, J., Oviatt, C.G.J., Nash, B., Duke, D., and Young, D.C., 2022, Building a master chronology for the western lake Bonneville basin with stratigraphic and elemental data from multiple sites, USA: Radiocarbon, v. 64, no. 1, p. 69–85, doi: 10.1017/RDC.2022.3.

Homewood, P., Mettraux, M., Vanden Berg, M., Foubert, A., Neumann, R., Newell, D., and Atwood, G., 2022, Onshore groundwater spring carbonate mounds to lacustrine microbialites, the perplexing record of a transitional Great Salt Lake carbonate shoreline at Lakeside, Utah: The Depositional Record, v. 8, no. 1, p. 9–38, doi: 10.1002/dep2.148.

Ingalls, M., Frantz, C.M., Snell, K.E., and Trower, E.J., 2020, Carbonate facies-specific stable isotope data record climate, hydrology, and microbial communities in Great Salt Lake, UT: Geobiology, v. 18, no. 5, p. 566–593, doi: 10.1111/gbi.12386.

Jones, B.F., Naftz, D.L., Spencer, R.J., and Oviatt, C.G., 2009, Geochemical Evolution of Great Salt Lake, Utah, USA: Aquatic Geochemistry, v. 15, no. 1–2, p. 95–121, doi: 10.1007/s10498-008-9047-y.

Kanik, M., Munro-Ehrlich, M., Fernandes-Martins, M.C., Payne, D., Gianoulias, K., Keller, L., Kubacki, A., Lindsay, M.R., Baxter, B.K., Vanden Berg, M.D., Colman, D.R., and Boyd, E.S., 2020, Unexpected Abundance and Diversity of Phototrophs in Mats from Morphologically Variable Microbialites in Great Salt Lake, Utah (H. Atomi, Ed.): Applied and Environmental Microbiology, v. 86, no. 10, p. e00165-20, doi: 10.1128/AEM.00165-20.

Kijowski, A.M., Neill, J., Wickline, A., Swift, J., Butler, J.K., Kimberly, D.A., Van Leeuwen, J., Luft, J., and Stone, K., 2020, American white pelicans of Gunnison Island, Great Salt Lake, Utah, *in* Baxter, B.K., and Butler, J.K., editors, Great Salt Lake Biology: A Terminal Lake in a Time of Change: Cham, Springer International Publishing, p. 311–344, doi: 10.1007/978-3-030-40352-2_10.

Lindsay, M.R., Anderson, C., Fox, N., Scofield, G., Allen, J., Anderson, E., Bueter, L., Poudel, S., Sutherland, K., Munson-McGee, J.H., Van Nostrand, J.D., Zhou, J., Spear, J.R., Baxter, B.K., and others, 2017, Microbialite response to an anthropogenic salinity gradient in Great Salt Lake, Utah: Geobiology, v. 15, no. 1, p. 131–145, doi: 10.1111/gbi.12201.

Lindsay, M.R., Johnston, R.E., Baxter, B.K., and Boyd, E.S., 2019, Effects of salinity on microbialite-associated production in Great Salt Lake, Utah: Ecology, v. 100, no. 3, doi: 10.1002/ecy.2611.

MacIntyre, S., and Melack, J.M., 1995, Vertical and horizontal transport in lakes: Linking littoral, benthic, and pelagic habitats: Journal of the North American Benthological Society, v. 14, no. 4, p. 599–615, doi: 10.2307/1467544.

Marden, B., Brown, P., and Bosteels, T., 2020, Great Salt Lake Artemia: Ecosystem functions and services with a global reach, *in* Baxter, B.K., and Butler, J.K., editors, Great Salt Lake Biology: A Terminal Lake in a Time of Change: Cham, Springer International Publishing, p. 175–237, doi: 10.1007/978-3-030-40352-2_7.

Newell, D.L., Jensen, J.L., Frantz, C.M., and Vanden Berg, M.D., 2017, Great Salt Lake (Utah) Microbialite δ^{13}C, δ^{18}O, and δ^{15}N Record Fluctuations in Lake Biogeochemistry Since the Late Pleistocene: Geochemistry, Geophysics, Geosystems, v. 18, no. 10, p. 3631–3645, doi: 10.1002/2017GC007078.

Null, S.E., and Wurtsbaugh, W.A., 2020, Water development, consumptive water uses, and Great Salt Lake, *in* Baxter, B.K., and Butler, J.K., editors, Great Salt Lake Biology: A Terminal Lake in a Time of Change: Cham, Springer International Publishing, p. 1–21, doi: 10.1007/978-3-030-40352-2_1.

Oviatt, C.G., 2015, Chronology of Lake Bonneville, 30,000 to 10,000 yr B.P.: Quaternary Science Reviews, v. 110, p. 166–171, doi: http://linkinghub.elsevier.com/retrieve/pii/0277379114005071.

Oviatt, C.G., Atwood, G., and Thompson, R.S., 2021, History of Great Salt Lake, Utah, USA: since the termination of lake Bonneville, *in* Rosen, M.R., Finkelstein, D.B., Park Boush, L., and Pla-Pueyo, S., editors, Limnogeology: Progress, Challenges and Opportunities : A Tribute to Elizabeth Gierlowski-Kordesch: Cham, Springer International Publishing Syntheses in Limnogeology, p. 233–271, doi: 10.1007/978-3-030-66576-0_8.

Pace, A., Bourillot, R., Bouton, A., Vennin, E., Galaup, S., Bundeleva, I., Patrier, P., Dupraz, C., Thomazo, C., Sansjofre, P., Yokoyama, Y., Franceschi, M., Anguy, Y., Pigot, L., and others, 2016, Microbial and diagenetic steps leading to the mineralisation of Great Salt Lake microbialites: Scientific Reports, v. 6, no. 1, p. 31495, doi: 10.1038/srep31495.

Paradis, O.P., Corsetti, F.A., Bardsley, A., Hammond, D.E., Berelson, W., Xu, X., Walker, J., and Celestian, A., 2023, Radiocarbon chronology/growth rates of ooids from Great Salt Lake, Utah, *in* Vanden Berg, M.D., Ford, R., Frantz, C., Hurlow, H., Gunderson, K., and Atwood, G. (eds.), Great Salt Lake and the Bonneville Basin: Geologic History and Anthropocene Issues: Utah Geological Association Publication 51, p. [PLACEHOLDER PENDING INFO FROM VOLUME].

Pedone, V.A., and Folk, R.L., 1996, Formation of aragonite cement by nannobacteria in the Great Salt Lake, Utah: Geology, v. 24, no. 8, p. 763-765, doi: 10.1130/0091-7613(1996)024<0763:FOACBN>2.3.CO;2.

Post, F.J., 1977, The microbial ecology of the Great Salt Lake: Microbial Ecology, v. 3, no. 2, p. 143–165, doi: 10.1007/BF02010403.

Shapiro, R.S., 2000, A comment on the systematic confusion of thrombolites: Palaios, v. 15, p. 166–169.

Shen, Y., Suarez-Gonzalez, P., and Reitner, J., 2022, Contrasting modes of carbonate precipitation in a hypersaline microbial mat and their influence on biomarker preservation (Kiritimati, Central Pacific): Minerals, v. 12, no. 2, p. 267-297, doi: 10.3390/min12020267.

Sorensen, E.D., Hoven, H.M., and Neill, J., 2020, Great Salt Lake Shorebirds,their habitats, and food base, *in* Baxter, B.K., and Butler, J.K., editors, Great Salt Lake Biology: A Terminal Lake in a Time of Change: Cham, Springer International Publishing, p. 263–309, doi: 10.1007/978-3-030-40352-2_9.

Utah DNR Forestry, 2013, Great Salt Lake comprehensive management plan: Utah Department of Natural Resources Division of Forestry, Fire & State Lands Record of Decision 13-0315–1, 391 p.

Vanden Berg, M.D., 2019, Domes, Rings, Ridges,

and Polygons: Characteristics of microbialites from Utah's Great Salt Lake (L. Birgenheier & H. Harper, Eds.): The Sedimentary Record, v. 17, no. 1, p. 4–10, doi: 10.2110/sedred.2019.1.4.

Vennin, E., Bouton, A., Bourillot, R., Pace, A., Roche, A., Brayard, A., Thomazo, C., Virgone, A., Gaucher, E.C., Desaubliaux, G., and Visscher, P.T., 2019, The lacustrine microbial carbonate factory of the successive Lake Bonneville and Great Salt Lake, Utah, USA (A. Brasier, Ed.): Sedimentology, v. 66, no. 1, p. 165–204, doi: 10.1111/sed.12499.

Virtanen, P., Gommers, R., Oliphant, T.E., Haberland, M., Reddy, T., Cournapeau, D., Burovski, E., Peterson, P., Weckesser, W., Bright, J., van der Walt, S. J., Brett, M., Wilson, J., Millman, K. J., Mayorov, N., Nelson, A. R. J., Jones, E., Kern, R., Larson, E., Carey, C. J., Polat, I., Feng, Y., Moore, E. W., VanderPlas, J., Laxalde, D., Perktold, J., Cimrman, R., Henriksen, I., Quintero, E. A., Harris, C. R., Archibald, A. M., Ribeiro, A. H., Pedregosa, F., van Mulbregt, P., and SciPy 1.0 Contributors, 2020, SciPy 1.0: Fundamental Algorithms for Scientific Computing in Python: Nature Methods, v. 17, no. 3, p. 261-272.

Wurtsbaugh, W.A., 2009, Biostromes, brine flies, birds, and the bioaccumulation of selenium in Great Salt Lake, Utah: Saline lakes around the world: unique systems with unique values. Natural Resources and Environmental Issues, vol XV, v. 15, p. 1–15.

Wurtsbaugh, W.A., Gardberg, J., and Izdepski, C., 2011, Biostrome communities and mercury and selenium bioaccumulation in the Great Salt Lake (Utah, USA): Science of The Total Environment, v. 409, no. 20, p. 4425–4434, doi: 10.1016/j.scitotenv.2011.07.027.

SUPPLEMENTARY INFORMATION

.

Mapped microbialite area shapefiles, data tables, Python code used for analysis, and supplemental figures are available at Open Science Framework: https://osf.io/uf9yg/.

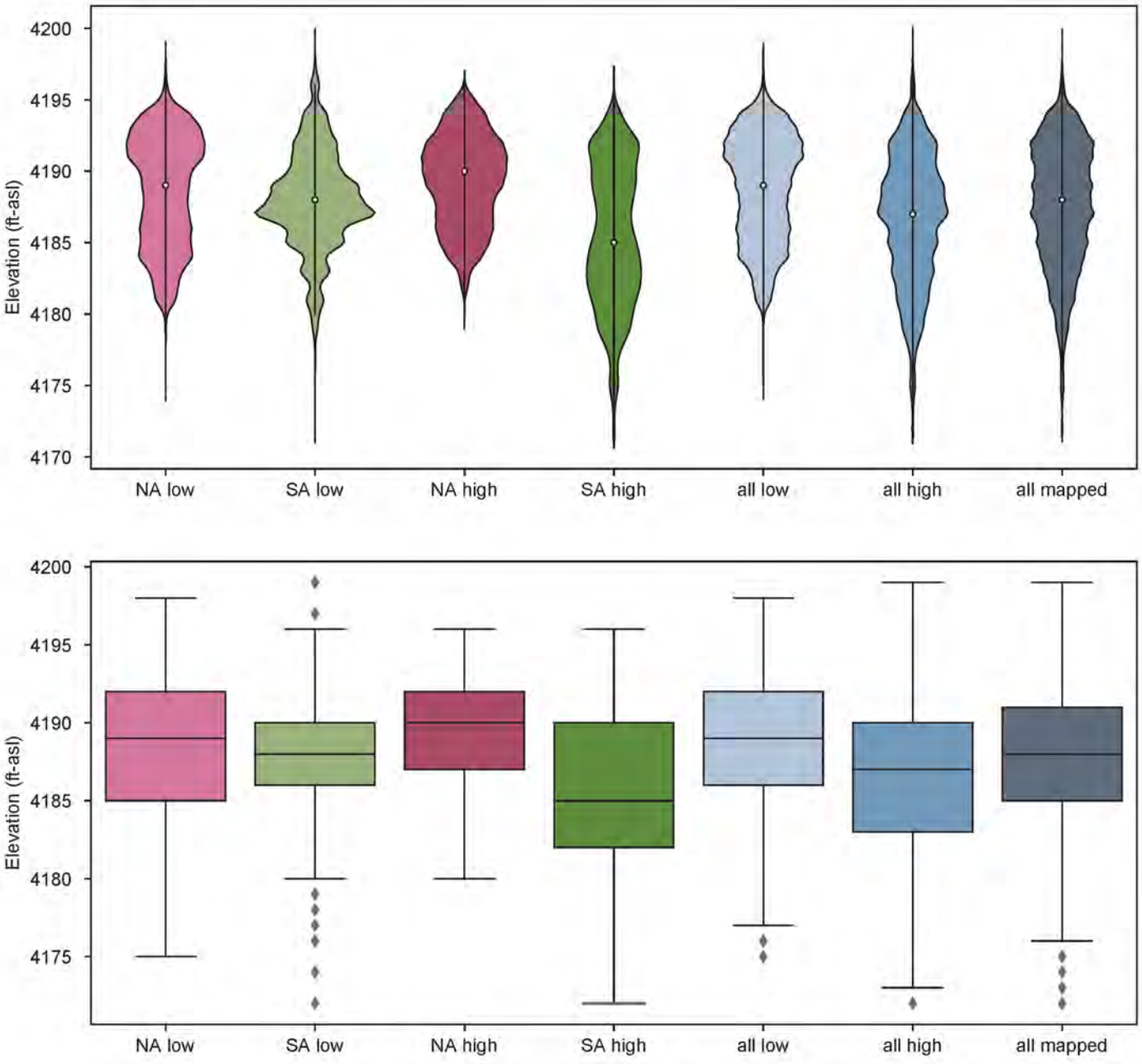

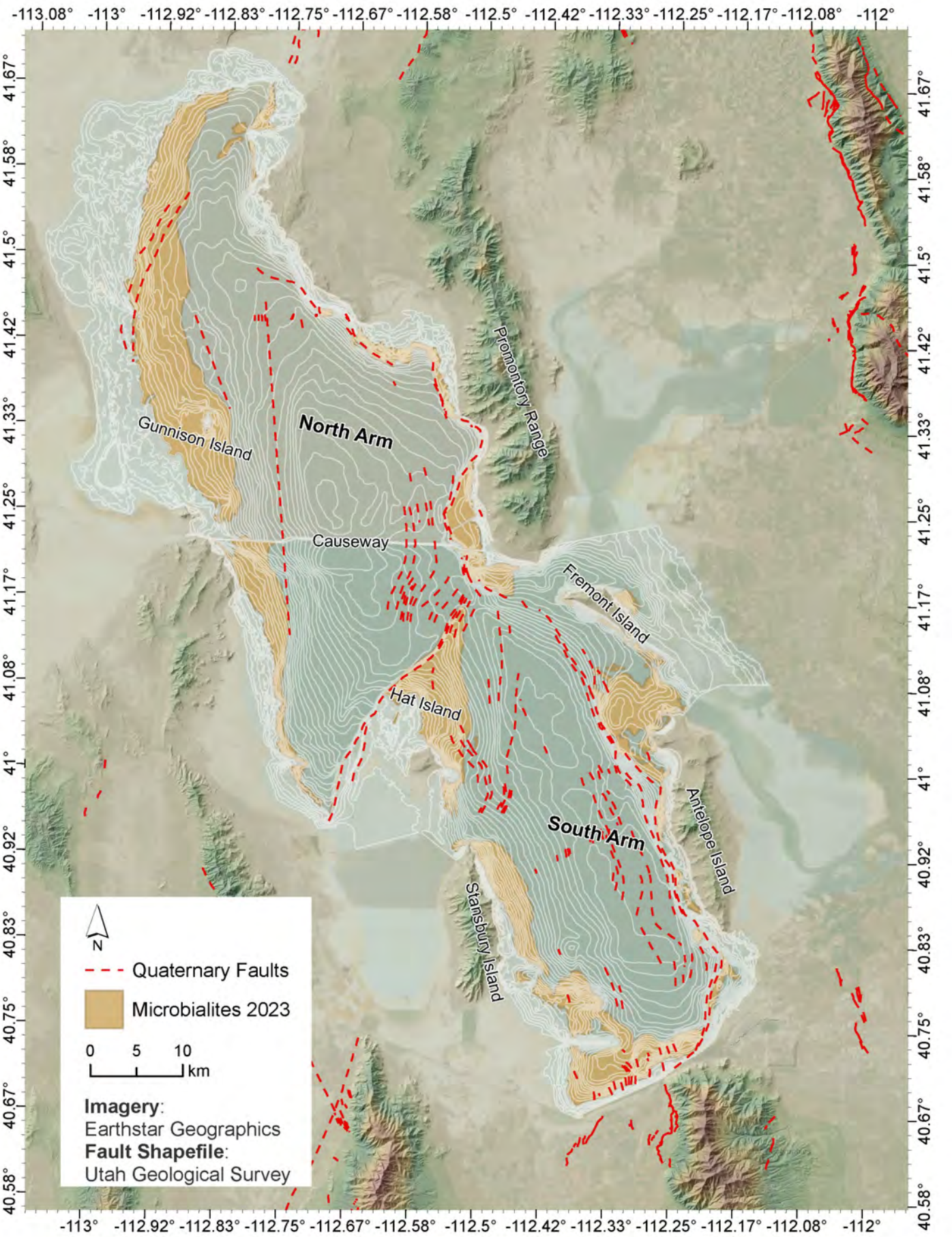
-113.08° -113° -112.92° -112.83° -112.75° -112.67° -112.58° -112.5° -112.42° -112.33° -112.25° -112.17° -112.08° -112°
41.67° 41.58° 41.5° 41.42° 41.33° 41.25° 41.17° 41.08° 41° 40.92° 40.83° 40.75° 40.67° 40.58°
Gunnison Island
North Arm
Promontory Range
Causeway
Fremont Island
Hat Island
South Arm
Antelope Island
Stansbury Island
N
Quaternary Faults
Microbialites 2023
0 5 10
km
Imagery:
Earthstar Geographics
Fault Shapefile:
Utah Geological Survey